The Astrophysical Journal, 944:2 (15pp), 2023 February 10 https://doi.org/10.3847/1538-4357/ac9bf9

Turbulent Magnetic Diffusivity β Effect in a Magnetically Forced System

Kiwan Park, Myung Ki Cheoun, and Chang-Bae Kim
Department of Physics and OMEG Institute, Soongsil University, 369, Sangdo-ro, Dongjak-gu, Seoul 06978, Republic of Korea; pkiwan@ssu.ac.kr
Received 2022 May 10; revised 2022 October 15; accepted 2022 October 18; published 2023 February 8

Abstract

We have studied the large-scale dynamo forced with helical magnetic energy. Compared to the kinetic forcing process, the magnetic process is not clearly observed nor intuitive. However, it may represent the actual B field amplification in the stellar corona, accretion disk, plasma lab, or other magnetically dominated systems where the strong kinetic effect does not exist. The interaction between the magnetic field and the plasma is essentially nonlinear. However, when the plasma system is driven by helical energy, whether kinetic or magnetic, the nonlinear process can be linearized with pseudotensors a, β and the large-scale magnetic field $\overline{\boldsymbol{B}}$. Conventionally, the α effect is thought to be the main dynamo effect converting kinetic energy into magnetic energy and transferring it to the large-scale regime. In contrast, β effect has been thought to diffuse magnetic energy. However, these conclusions are not based on the exact definition of α and β. In this paper, instead of the analytic definition of α and β, we derive a semi-analytic equation and apply it to the simulation data. The half analytic and numerical result shows that the averaged α effect is not so important in amplifying the $\overline{\boldsymbol{B}}$ field. Rather, it is the negative β effect combined with the Laplacian ($\nabla^2 \rightarrow -k^2$) that plays a key role in the dynamo process. Further, the negative magnetic diffusivity accounts for the attenuation of the plasma kinetic energy $\overline{E}_V$ in large scales. We discuss this process using the theoretical method and the intuitive field structure model.

Unified Astronomy Thesaurus concepts: Solar dynamo (2001); Magnetohydrodynamics (1964); Magnetic fields (994); Plasma astrophysics (1261)

1. Introduction

Most celestial plasma systems are constrained by a magnetic field B. The B field takes energy from the turbulent plasma, and the amplified field back reacts to the system constraining its evolution. However, the role of the B field, as well as its evolving process, is not yet completely understood. Briefly, it controls the rate of formation of a star and accretion disk (Balbus & Hawley 1991; Machida et al. 2005). Further, the balanced pressure between the magnetic field and plasma can decide the stability of the system (see the sausage, kink, or Kruskal–Schwarzschild instabilities; see Boyd & Sanderson 2003).

The amplification of the magnetic field (dynamo) includes the conversion of kinetic energy into magnetic energy and its transport in the plasma system. The converted B field cascades toward a large-scale regime or a small-scale one, both of which are essentially inducing the B field through the electromotive force (EMF; $\nabla \times (\boldsymbol{U} \times \boldsymbol{B})$, $\boldsymbol{U}$: fluidic velocity). The migration of magnetic energy toward the large-scale regime is called "inverse cascade" and leads to a large-scale dynamo (LSD), whereas that toward the small-scale regime is called "cascade of energy" and leads to a small-scale dynamo (SSD). The cascade of energy toward the smaller scale is often found in hydrodynamics (HD) and magnetohydrodynamics (MHD). However, the inverse cascade of energy requires more constrained conditions.

Statistically, in the case of (quasi) two-dimensional HD, the inverse cascade of energy occurs with the conserved kinetic energy $\langle U^2 \rangle/2$ and enstrophy $\langle \omega^2 \rangle$ ($\omega = \nabla \times \boldsymbol{U}$; Davidson 2004). For two-dimensional MHD, the total energy $\langle U^2 + B^2 \rangle/2$, cross helicity $\langle \boldsymbol{U} \cdot \boldsymbol{B} \rangle$, and squared vector potential $\langle A^2 \rangle$ should be conserved. In three-dimensional MHD, magnetic helicity $\langle \boldsymbol{A} \cdot \boldsymbol{B} \rangle$, which is essentially conserved, is necessary instead of the vector potential (Moffatt 1978; Krause & Rädler 1980). However, in the decaying MHD system without any energy source, magnetic energy migrates to the large-scale regime regardless of the constraints (Ditlevsen et al. 2004; Brandenburg et al. 2015; Park 2017; Brandenburg & Kahniashvili 2017, and references therein). Brandenburg & Kahniashvili (2017) numerically investigated the motion of kinetic energy in a decaying HD system compared with that of the (non)helical magnetic energy in decaying MHD systems. In the HD system, no actual inverse transfer of kinetic energy was observed. However, in the MHD system, the magnetic energy was inversely transferred regardless of the magnetic helicity. The inverse transfer of the decaying helical magnetic energy can be explained with the a effect (Park 2017), but that of the nonhelical case is not yet clearly understood. Nonetheless, the unusual expansion of the magnetic scale in the decaying plasma system may explain one of the origins of the large-scale magnetic fields that ubiquitously exist in space where no specific energy source or helicity exist.

In addition to the energy migration, the dynamo can be categorized into a kinetic forcing dynamo (KFD) and a magnetic forcing dynamo (MFD) according to the type of forcing energy. KFD is the conventional dynamo process that converts kinetic energy into magnetic energy. In MFD, however, the conversion of kinetic energy to magnetic energy is not the main process. Instead, the externally supplied magnetic energy migrates (evolves) in the plasma through EMF with the help of kinetic energy. Compared with KFD, MFD is the result of electromagnetic (EM) phenomena that are ubiquitous in the space plasma system. The evolution of the magnetic field in the plasma is described by the magnetic

induction equation derived from Faraday's law, $\partial \boldsymbol{B}/\partial t = -\nabla \times \boldsymbol{E}$, and (generalized) Ohm's law, the $\boldsymbol{J} = \boldsymbol{E} + \boldsymbol{U} \times \boldsymbol{B}\,(+\boldsymbol{F})$ (η: magnetic diffusivity). As these equations show, the direct supply of electromagnetic energy or any force such as the Hall effect or radiation that yields a current density can produce a magnetic field. For example, the origin of a $\boldsymbol{B}$ field in the plasma lab, including a reversed field pinch (RFP; Marrelli et al. 2021), is electromagnetic rather than kinetic. Additionally, the effect of the electric force, gravitational force, or inhomogeneously distributed B field can yield various drift motions of the charged particles. In the accretion disk, the magnetic field not only transfers angular momentum but also drives the plasma particles through the Lorentz force to induce nontrivial EMF and subsequent magnetic fields. Turbulent kinetic energy by itself cannot be transferred to such a huge distance to keep the shape of the jet in an active galactic nucleus.

When the field is helical ($\nabla \times \boldsymbol{B} = \lambda \boldsymbol{B}$), regardless of KFD or MFD, turbulent EMF $\langle \boldsymbol{u} \times \boldsymbol{b} \rangle$ can be replaced with $\alpha \overline{\boldsymbol{B}} - \beta \nabla \times \overline{\boldsymbol{B}}$.[1] Conventionally, it has been thought that the α effect amplifies the magnetic energy and the β effect diffuses it. However, this conclusion is not based on precise values of a and β. Strictly speaking, their exact definitions are not yet known. Only their sketchy representations can be derived from dynamo theories, such as the mean field theory (MFT; Moffatt 1978), eddy damped quasi-normal markovianized approximation (EDQNM; Pouquet et al. 1976), or direct interactive approximation (DIA; Yoshizawa 2011). They commonly show that α is composed of the current helicity and kinetic helicity ($\sim \langle \boldsymbol{b} \cdot \nabla \times \boldsymbol{b} \rangle - \langle \boldsymbol{u} \cdot \nabla \times \boldsymbol{u} \rangle$). The β effect is a function of the turbulent energy $\sim \langle u2 \rangle (+ \langle b^2 \rangle)$. As the definition of α implies, there is no constraint between the helical kinetic energy "$-\langle \boldsymbol{u} \cdot \nabla \times \boldsymbol{u} \rangle$" and the helical magnetic energy "$\langle \boldsymbol{b} \cdot \nabla \times \boldsymbol{b} \rangle$" in forcing $\overline{\boldsymbol{B}}$. A helical magnetic forcing dynamo (HMFD) as well as a helical kinetic forcing dynamo (HKFD) can be feasible independent dynamo processes. Finding a and β in HMFD is the aim of our work.

In HMFD, there are a couple of things to be made clear. α should be larger than the dissipation rate for a magnetic field to arise. If the current helicity is a unique component in the α effect, the magnetic field grows without stopping. To prevent this catastrophic amplification, there should be sort of a constraining effect, such as that of the kinetic helicity, as HKFD assumes ($\langle \boldsymbol{u} \cdot \omega \sim \langle \boldsymbol{j} \cdot \boldsymbol{b} \rangle$). However, as the helical magnetic field nullifies the Lorentz force $\boldsymbol{J} \times \boldsymbol{B}$ on average, the generation of a helical velocity field by the helical $\boldsymbol{B}$ field looks contradictory. Moreover, there are tricky issues in the conservation and polarization of helicity. If the system is forced by right-handed helical kinetic energy, left-handed magnetic helicity is generated and inversely cascaded. At the same time, right-handed magnetic helicity is generated in the small-scale regime to conserve the magnetic helicity in the system. In HMFD, however, right-handed magnetic helicity is generated in the entire system (Park & Blackman 2012a, 2012b). The physical influence of magnetic polarization on the plasma system is not yet well understood.

On the other hand, for the amplification of the B field in the plasma, the seed magnetic field B_0 is not absolutely necessary in MFD. However, we briefly introduce its origin in space because B_0 is indispensable to KFD and decides the field profiles in the decaying MHD system. Its cosmological origins are divided into the era of inflationary genesis and post-inflationary magnetogenesis. The first inflationary scenario generates the very-large-scale PMF, but it needs the breaking of conformal symmetry by the interaction of the electromagnetic field and the gravitational field. The breaking of the conformal symmetry is to consider the electromagnetic coupling to the scalar field (Martin & Yokoyama 2008; Subramanian 2016), coupling to the modified general relativity theory, coupling to the pseudoscalar field, and so on. The PMF strength could be generated by quantum fluctuations and has been estimated to be 10^{-5}–1 Mr (Yamazaki et al. 2012). The generated magnetic field via the inflation process could in principle be scale-invariant with $P(k) \sim k^{-3}$ and more stable on large scales. However, on scales larger than the Hubble scale, the correlation cannot be expected by causality. Here, we note that a superhorizon (inhomogeneous) PMF model generated from the fluctuations of the magnetic field has been suggested to explain the Bing Bang nucleosynthesis (Demozziet al. 2009; Luo et al. 2019).

The second scenario is based on the cosmological quantum chromo dynamics (QCD) phase transition (∼250 MeV; Cheng & Olinto1994; Tevzadze et al. 2012) and the electroweak phase transition (∼100 MeV). The PMF could be generated by the collision and percolation of some bubbles from the first-order transition and is estimated to be 10^{-7} nG by the quark-hadron and 10^{-14}–10^{-8} nG by the electroweak transition. The second scenario of phase transition includes the violent processes of separating the charges and yielding the turbulent fluid motion. First-order phase transition occurs through bubble nucleation, whose correlation length is finite and a fraction of the Hubble scale (Ahonen & Enqvist 1998). The scale of the magnetic field generated at the second-order phase transition would be much shorter and damped by ohmic dissipation. Therefore, the phase transition was argued only to explain the small-scale amplification of the comoving magnetic field and the limited correlation length scale, not for a large-scale magnetic field such as the magnetic field in galaxies or clusters of galaxies (Vachaspati 2021). However, we note that a recent simulation of the magnetic field employing the decaying turbulence at the phase (first-order) transition illustrates the appearance of a strong comoving magnetic field much larger than 1 μG with a relatively larger correlation length and the possibility of a gravitational wave signal from the strong turbulent source (Kahniashvili et al. 2022). The magnetic field produced through causal processes at phase transitions might serve as a seed for the fields observed in galaxies and clusters.

The third scenario can occur during or after the epoch of photon scattering. The PMF can be produced by nonvanishing vorticity, which arises from the nonzero electron and proton fluid angular velocities by the different masses of proton and electron in the gravitational field (Harrison mechanism; Harrison 1970). The PMF is thought to be about 10^{-9} Mr. However, the strength of B_0 inferred from these quantum fluctuations is too small to account for the KFD seed field. So, another amplification process that connects PMF and KFD must have existed.

The second and third scenarios are thought to occur on a correlation scale smaller than the Hubble radius, for which we expect a suitable field generated by another dynamical effect such as the Biermann battery mechanism (Schluter 1950). When the hot ionized particles (plasma) collide, the fluctuating

[1] We decomposed field $\boldsymbol{X}$ into the large-scale quantity $\overline{\boldsymbol{X}}$ and turbulent quantity $\boldsymbol{x}$.

electron density ∇n_e and pressure ∇p_e (or temperature ∇T_e) can be misaligned. This instability, $-\nabla p_e/(n_e e)$, can drive currents to generate magnetic fields. This is a typical example of a nonhelical magnetic forcing dynamo. Moreover, the cosmological density fluctuations by second-order couplings between photons and electrons, which can involve anisotropic pressure of photons pushing electrons in directions different to the protons (Ichiki et al. 2006), can produce the large-scale magnetic fields as well as large-scale structures in the universe. Further, the neutrino interaction with charged leptons at the early epoch is thought to have generated primordial magnetic helicity in addition to the well-known ponderomotive electric force (Semikoz & Sokoloff 2005). As the electric field in Faraday's law is replaced by EMF and current density, the neutrino–lepton interaction can yield the modified magnetic induction equation, i.e., it is one of the promising candidates of magnetic field generation. These two processes are typical examples of MFD (see the Appendix).

Besides, in space, the guide magnetic field $B_{\rm ext}$ is mixed with the self-generated B field and affects the overall evolution of the plasma system. The effect of $B_{\rm ext}$ can be described by the Elsässer variable ($z^{\pm} = v \pm b$) equation (Elsässer 1950; Biskamp 2005):

$$\frac{\partial z^{\pm}}{\partial t} \mp v_A \cdot \nabla z^{\pm} + z^{\mp} \cdot \nabla z^{\pm} = -\nabla P + \frac{1}{2}(\nu + \eta)\nabla^2 z^{\pm} + \frac{1}{2}(\nu - \eta)\nabla^2 z^{\mp} + f^{\pm}, \quad (1)$$

where $v_A = B_{\rm ext}/\sqrt{\mu_0 \rho_0}$ (μ_0: magnetic permeability, ρ_0: density of charged particle) is the Alfvén velocity. The ratio between $v_A \cdot \nabla z^{\pm}$ and $z^{\mp} \cdot \nabla z^{\pm}$ decides the profile of the energy spectrum. The strong linear effect due to $B_{\rm ex}$ suppresses the plasma motion leading to weak turbulence (Galtier et al. 2000).

$$v_A \cdot \nabla z^{\pm} \gg z^{\mp} \cdot \nabla z^{\pm} \rightarrow k_{\parallel} v_A \gg k_{\perp} b_{\perp}. \quad (2)$$

($k_{\parallel}$ is the wavenumber parallel to the guide field. $k_{\perp}$ and $b_{\perp}$ are the wavenumber and magnetic fluctuation perpendicular to the guide field, respectively). In contrast, if the nonlinear effect is dominant, the effect of turbulence increases (Goldreich & Sridhar 1995), and if the guide magnetic field is much weaker than the dynamo-generated magnetic field, the effect of the guide magnetic field decreases. However, regardless of "v_A," the effect of turbulence grows in proportion to the wavenumber $k_{\perp}$.

So far, we have briefly introduced the type of dynamo including the α and β effects, seed field effect, and effect of guiding magnetic field. However, in this paper, we mainly study α and β in HMFD. We derive their indirect representations as functions of the large-scale magnetic energy and helicity (Park 2020). Applying simulation data to the semi-analytic theory, we study the evolving profiles of α and β. Followed by this introductory section, the numerical method and related MHD equations for simulation are discussed in Section 2. In Section 3, we show the numerical results for the evolving B field and its inverse cascade to the large-scale regime. Then, we show the evolving profiles of α and β along with the growth of the B field and investigate their physical features and mutual relations. Moreover, we verify the results with simulation and analytic proof. In Section 4, we discuss the parameterisations of EMF with α and β and compare them using numerical data and an analytic approach. Using the field structure model, we explain the intuitive meaning of theα effect and how β becomes negative. Then, we rederive the β coefficient when the field is helical. The β effect also explains how the plasma velocity field is suppressed when the system is forced by a helical magnetic field. This work focuses on the physical mechanism of a helical forcing dynamo, which occurs in the fundamental level of astroplasma systems. In Section 5, we summarize our work.

2. Numerical Method

The dynamo phenomenon can be explained with the MHD model. The basic MHD equations are composed of the continuity, momentum, and magnetic induction equations as follows:

$$\frac{\partial \rho}{\partial t} = -\boldsymbol{U} \cdot \boldsymbol{\nabla}\rho - \rho \boldsymbol{\nabla} \cdot \boldsymbol{U}, \quad (3)$$

$$\frac{\partial \boldsymbol{U}}{\partial t} = -\boldsymbol{U} \cdot \boldsymbol{\nabla}\boldsymbol{U} - \boldsymbol{\nabla} \ln \rho + \frac{1}{\rho}\boldsymbol{J} \times \boldsymbol{B} + \nu\left(\boldsymbol{\nabla}^2 \boldsymbol{U} + \frac{1}{3}\boldsymbol{\nabla}\boldsymbol{\nabla} \cdot U\right) + \boldsymbol{f}_{\rm kin}, \quad (4)$$

$$\frac{\partial \boldsymbol{A}}{\partial t} = \boldsymbol{U} \times \boldsymbol{B} - \eta \nabla \times \boldsymbol{B} + \boldsymbol{f}_{\rm mag}. \quad (5)$$

$$\left(\Rightarrow \frac{\partial \boldsymbol{B}}{\partial t} = \nabla \times (\boldsymbol{U} \times \boldsymbol{B}) + \eta \nabla^2 \boldsymbol{B} + \nabla \times \boldsymbol{f}_{\rm mag}\right). \quad (6)$$

Here, symbols ρ, ν, and η indicate the density, kinematic viscosity, and magnetic diffusivity. "$\boldsymbol{U}$" is in units of the sound speed, c_s, and "$\boldsymbol{B}$" is normalized by $(\rho_0\ \mu_0)^{1/2} c_s (m_0$: magnetic permeability in vacuum. The variables in these equations are unitless.)

These equations are solved theoretically or numerically. For the theoretical analysis, Fourier-transformed equations, which can be solved algebraically, are used for the detailed calculation of the entire scale. However, in many cases, a simple two- or three-scale model is often used to investigate the most characteristic properties. For example, $\boldsymbol{U}$ and $\boldsymbol{B}$ in Equation (6) are separated into the large-scale fields $\overline{\boldsymbol{U}}$ and $\overline{\boldsymbol{B}}$ and turbulent small-scale fields $\boldsymbol{u}$ and $\boldsymbol{b}$. Then, the $\overline{\boldsymbol{B}}$ field evolves with

$$\frac{\partial \overline{\boldsymbol{B}}}{\partial t} = \nabla \times \langle \boldsymbol{u} \times \boldsymbol{b} \rangle + \eta \nabla^2 \overline{\boldsymbol{B}}. \quad (7)$$

The forcing function "$\boldsymbol{f}$" is usually applied to the small-scale regime so that its effect is included in "$\boldsymbol{u}$" or "$\boldsymbol{b}$." That is, EMF contains the forcing effect implicitly. Additionally, when the field is helical, this equation can be represented with a more simplified form as follows (Pouquet et al. 1976; Park & Blackman 2012a):

$$\frac{\partial \overline{\boldsymbol{B}}}{\partial t} \sim \alpha \underbrace{\nabla \times \overline{\boldsymbol{B}}}_{\overline{\boldsymbol{J}}} + (\beta + \eta)\nabla^2 \overline{\boldsymbol{B}}. \quad (8)$$

Physically, this equation means that the magnetic field is induced by the current density (Ampere's law) with α and plasma fluidic diffusion with β. These pseudoscalar tensors can be derived with MFT, DIA, or EDQNM. However, no exact theoretical method has been found yet. We do not discuss any rigorous way to derive the pseudoscalars in this paper. Instead,

we suggest a detour approach to obtain their temporal evolving profiles with numerical simulation.

For the numerical simulation, we used the Pencil Code (Brandenburg 2001) to solve Equations (3)–(5). The Pencil Code is a sixth-order finite-difference code for compressible fluid dynamics accounting for the magnetic field. The code solves for the vector potential "$\boldsymbol{A}$" in Equation (5) instead of the magnetic field "$\boldsymbol{B}$" in Equation (6). Solving for "$\boldsymbol{A}$," the condition of a divergence-free magnetic field ($\nabla \cdot \boldsymbol{B} = 0$) is met without numerical manipulation. Moreover, the magnetic helicity $H_M(=\langle \boldsymbol{A}\cdot\boldsymbol{B}\rangle)$ as well as the magnetic energy $E_M(=\langle B^2/2\rangle)$ can be calculated free from the gauge issue with the assumption of the simply connected volume.

To drive a dissipative plasma system, we used a forcing function like

$$\boldsymbol{f}_{\rm mag}(k,\,t) = \frac{i\boldsymbol{k}(t)\times(\boldsymbol{k}(t)\times\hat{\boldsymbol{e}}) - \lambda|\boldsymbol{k}(t)|(\boldsymbol{k}(t)\times\hat{\boldsymbol{e}})}{k(t)^2\sqrt{1+\lambda^2}\sqrt{1-(\boldsymbol{k}(t)\cdot\boldsymbol{e})^2/k(t)^2}}. \quad (9)$$

This is the Fourier-transformed function represented by a wavenumber "k," helicity ratio controller λ, and arbitrary unit vector "$\hat{\boldsymbol{e}}$." Simple calculations show that $\boldsymbol{f}_{\rm mag}$ is solenoidal: $\nabla\cdot\boldsymbol{f}\rightarrow i\boldsymbol{k}\cdot\boldsymbol{f}=0$ with a unit magnitude, $|f_{\rm mag}|=1$. Its second-order correlation is 1 regardless of λ: $\langle f^{*}f\rangle = (a2 + \lambda^2 b^2)/c^2 = 1$, where $\boldsymbol{a}=\boldsymbol{k}\times(\boldsymbol{k}\times\hat{\boldsymbol{e}})$, $\boldsymbol{b}=k(\boldsymbol{k}\times\hat{\boldsymbol{e}})$, and $\boldsymbol{c}=k^2\sqrt{1+\lambda^2}\sqrt{1-(\boldsymbol{k}\cdot\hat{\boldsymbol{e}})^2/k^2}$. Further, if λ is $+(-)1$, the forcing function generates a fully right-handed (left-handed) helical field: $\nabla\times\boldsymbol{f}_{\rm mag}\rightarrow i\boldsymbol{k}\times\boldsymbol{f}_{\rm mag}=\pm k\boldsymbol{f}_{\rm mag}$ and $\boldsymbol{f}_{\rm mag}\cdot\nabla\times\boldsymbol{f}_{\rm mag}\rightarrow\pm kf_{\rm mag}^2$. In contrast, $\lambda=0$ yields a nonhelical forcing field, and $0<|\lambda|<1$ yields the fractional helical field.

The numerically calculated data from this function are inversely Fourier transformed, $\boldsymbol{f}(\boldsymbol{r},\,t) = {\rm Re}(N\boldsymbol{f}_{{\rm mag},k(t)}\exp[i\boldsymbol{k}(t)\cdot\boldsymbol{r} + i\phi(t)])$, and attached to Equation (4) (KFD), or Equation (5) (MFD).[2] Here, $\boldsymbol{k}(t)=(k_x,\,k_y,\,k_z)$, and $\phi(t)$ is a random phase with $|\phi|<\pi$. N is a normalization factor $\sim c_s(kc_s/\delta t)^{1/2}$, where c_s and δt are the sound speed and time step, respectively. In each time step, a k value out of 350 vectors ($4.5<|k|<5.5$) is randomly chosen, and the forcing function becomes delta correlated in time.[3] These features of the forcing function are reflected in "U" and "B" in the plasma system characterized by viscosity, magnetic diffusivity, and other physical properties. We will discuss the helical stochastic effects reflected in α and β, which are in fact the second-order correlations of "U" and "B."

However, this forcing source cannot be compared with the real forcing source in nature. This function is specified for the investigation of the effect of helicity on the plasma system. It can be used as the kinetic forcing source $f_{\rm kin}$ or magnetic forcing source $f_{\rm mag}$. In the Appendix, we explained the theoretical background of MFD with two more realistic examples of $f_{\rm mag}$: the Biermann battery effect and neutrino–lepton interaction. One of the most essential differences between them is the magnetic helicity, which decides the direction of magnetic energy transfer.

[2] "$k(=2\pi/l)$" is inversely proportional to the eddy scale "l." $k=1$ indicates the largest scale, and the regime with $k\geqslant 2$ is considered as a small-scale (turbulent) regime.

[3] For the detailed properties of the forcing function, please refer to the Pencil Code manual in http://pencil-code.nordita.org/doc.php.

We gave the helical magnetic field (energy) at the randomly chosen wavenumber k, which is constrained by $\langle k\rangle_{\rm ave}\equiv k_f\sim 5$.

For both systems we used a unit magnetic Prandtl number $Pr_M = h/n = 1$. $h=n=6\times10^{-3}$, and the numerical resolution is 320^3. The systems were forced by Equation (9) with a fully helical magnetic field ($\lambda=+1$ or -1 at $k=5$). We used the basic data set of the kinetic energy $E_V(=\langle U^2\rangle/2)$, magnetic energy $E_M(=\langle B^2\rangle/2)$, kinetic helicity $\langle\boldsymbol{U}\cdot\nabla\times\boldsymbol{U}\rangle$, and magnetic helicity $\langle\boldsymbol{A}\cdot\boldsymbol{B}\rangle$. These data are produced by a default option, whose reliability has been verified. The magnetic vector potential generating the numerical seed field is of a smoothed random Gaussian field. It is spatially delta correlated with the initial profile of $E(k)\sim k^4$ and a decline at large wavenumbers. Its initial magnitude is 10^{-4} (Brandenburg 2001).

3. Numerical Results

The system in Figure 1(a), (c) is forced by a fully positive (right-handed) helical magnetic field (red dashed line; helicity ratio of forcing energy: $f_h\equiv k_f\langle\boldsymbol{a}\cdot\boldsymbol{b}\rangle/\langle b^{\,2}\rangle=1$, $k_f=5$ forcing wavenumber). In contrast, the system in Figure 1(b), (d) is forced by a fully negative (left-handed) magnetic helicity ($f_h=-1$). The peak speed U is $\sim 2\times10^{-3}$, and the magnetic Reynolds number is defined as ${\rm Re}_M\equiv UL/\eta\sim 2\pi/3$, where $L=2\,p$ and $h=6\times10^{-3}$. In HMFD, the least amount of magnetic energy is transferred to the plasma, and energy dissipation by viscous turbulence is minimum. This eccentric property leads to a low ratio of advection to diffusion ${\rm Re}_M$. If ${\rm Re}_M$ is redefined as "(turbulent) $f_{\rm mag}/\eta\nabla^2 B$," ${\rm Re}_M$ increases. However, we use the conventional definition in this manuscript.

In Figure 1(a), the large-scale magnetic energy $\langle\overline{B}^2\rangle$ ($=2\overline{E}_M$, $k=1$; solid line) grows to be saturated at $t\sim100$. Along with $\langle\overline{B}^2\rangle$, the large-scale magnetic helicity $\langle\overline{\boldsymbol{A}}\cdot\overline{\boldsymbol{B}}\rangle$ (dashed line) evolves keeping the relation of $\langle\overline{B}^2\rangle\geqslant k\langle\overline{\boldsymbol{A}}\cdot\overline{\boldsymbol{B}}\rangle$ ($k=1$). Moreover, the kinetic energy $\langle\overline{U}^2\rangle$ in the large scale grows keeping $\langle\overline{U}^2\rangle\geqslant\langle\overline{\boldsymbol{U}}\cdot\nabla\times\overline{\boldsymbol{U}}\rangle/k$. However, the direction of the kinetic helicity fluctuates from positive to negative as the discontinuous cusp line implies in this log-scaled plot. Similarly, Figure 1(c) shows the evolution of the small-scale magnetic energy $\langle b^2\rangle$ and kinetic energy $\langle u^2\rangle$ with their helical part $\langle\boldsymbol{u}\cdot\nabla\times\boldsymbol{u}\rangle/k$ and $k\langle\boldsymbol{a}\cdot\boldsymbol{b}\rangle$ ($k\geqslant2$). The fields grow and get saturated like the large-scale field, but the saturation occurs earlier because of their smaller eddy turnover time. The inverse cascade of magnetic energy from the forcing scale clearly shows up so that $\langle\overline{B}^2\rangle$ surpasses $\langle b^2\rangle$. This is a typical property of a helical large-scale dynamo.

Figures 1(b), (d) show the growth of the kinetic and magnetic energies in the system forced by the fully left-handed magnetic energy. Basically, they evolve consistently in comparison with Figures 1(a), (c). However, the kinetic helicity and magnetic helicity are invisible in this logarithmic plot indicating their left-handed (negative) chirality. The direction of helicity in the magnetically forced system tends to be consistent with that of the forcing energy. This is the opposite tendency of a helical kinetic forcing dynamo (HKFD). Nonetheless, the practically same growth in energy shows that the chirality of the forcing energy is not a determinant to the evolution of the plasma system.

Figure 2 shows the evolving magnetic helicity ratio $f_h\equiv k\langle\boldsymbol{a}\cdot\boldsymbol{b}\rangle/\langle b^2\rangle$ and kinetic helicity ratio $\langle\boldsymbol{u}\cdot\nabla\times\boldsymbol{u}\rangle/k\langle u^2\rangle$ for k=1, 5, 8. The left and right panels are for the right-handed forcing case (f_h=1, $\lambda=+1$ in Equation (9)) and left-handed

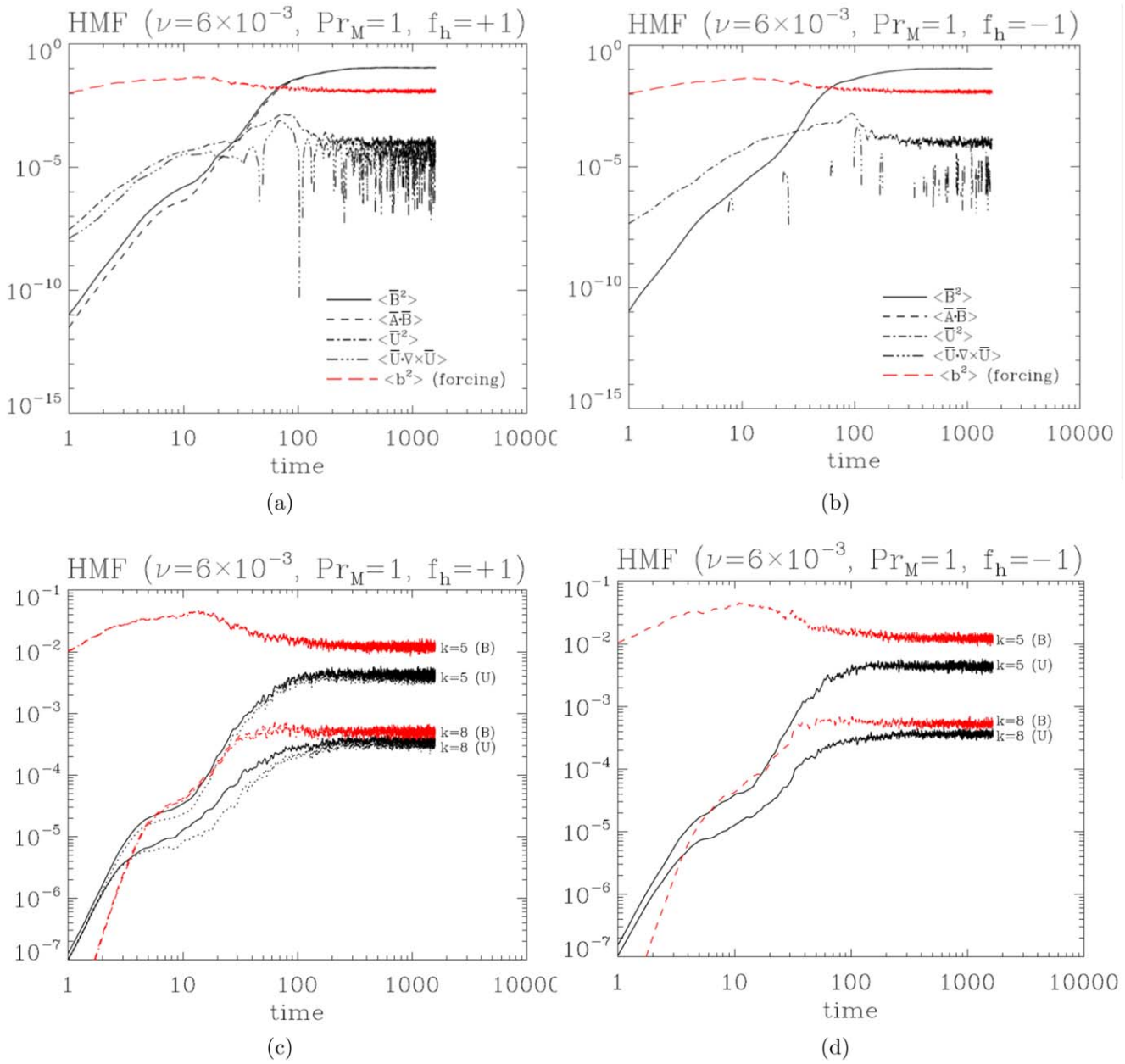

Figure 1. (a) and (c) Logarithmic evolution of the energy and helicity of the system forced with a right-handed helical magnetic field ($f_h = +1$).(b),(d)same as (a)and (c), but the system was forced with a left-handed helical magnetic field ($f_h = -1$). In (c), (d), $k = 5$ indicates the forcing scale eddy, and $k = 8$ indicates one of the small-scale ones. The red dashed line marks the magnetic energy $\langle b^2 \rangle$, and the red dotted line denotes its helical contribution $k\langle \boldsymbol{a} \cdot \boldsymbol{b} \rangle$. Here,$u$ and b represent the turbulent scale regime. Symbols (B) and (U) indicate the magnetic field and velocity field. In the forcing scale (k = 5), the magnetic energy and its helical part are practically the same so the corresponding lines overlap. On the other hand, the black solid line indicates the kinetic energy $\langle u^2 \rangle$, and the black dotted line indicates its helical part $\langle \boldsymbol{u} \cdot \nabla \times \boldsymbol{u} \rangle / k$ (different from (a), (b)). In (a) and (c), the kinetic helicity and magnetic helicity clearly show up, but those in (b) and (d) are not shown except some part of the large-scale kinetic helicity. This indicates that the polarization of the helicity in HMFD, except for the large-scale velocity, is consistently decided by the forcing magnetic field.

one ($f_h = -1$, $\lambda = -1$), respectively. The helicity ratio of the large-scale $\overline{B}$ is eventually saturated at $f_h = +1$ (-1), and that of the small-scale u and b reaches values lower (larger) than "1 (-1)." However, the helicity ratio of $\overline{U}$ can be as low as $\sim$0.25 (-0.25). A magnetic helicity ratio of less than "1" in the small-scale regime shows that the small-scale magnetic field substantially accelerates the large-scale plasma motion. Plasma in the large-scale regime is driven by the Lorentz force $\boldsymbol{J}(p) \times \boldsymbol{B}(q)$, where the wavenumbers are constrained by $p + q = 1$. This implies that the eddies associated with p, q are very close to each other in the small-scale regime and nearly out of phase. Helicity ratios smaller than 1 imply that the Lorentz force driving the large-scale eddy meaningfully grows: $\langle \boldsymbol{j} \times \boldsymbol{b} \rangle \neq 0$. However, the effect of the large-scale magnetic field on the plasma is limited: $\langle \overline{\boldsymbol{J}} \times \overline{\boldsymbol{B}} \rangle \sim 0$. Note that if we take the average of the Lorentz force in the entire scale, $\langle \boldsymbol{J} \times \boldsymbol{B} \rangle \sim 0$ due to the relative difference in the amplitude and eddy turnover time among scales. However, what arouses the plasma motion is the nontrivial $\langle \boldsymbol{j} \times \boldsymbol{b} \rangle$. The word "force free" for the helical field should not be confused.

The saturated helicity ratio "$f_h = 1$" for the large-scale field indicates that k for $\overline{\boldsymbol{B}}$ is definitely "1." Further, the initial

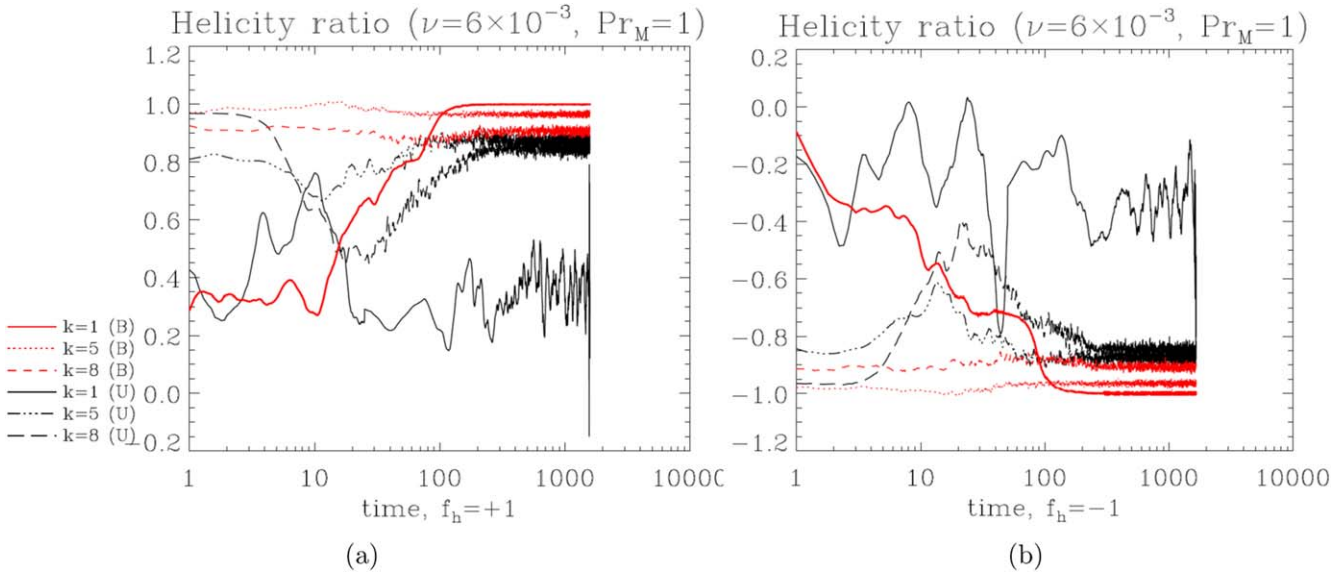

Figure 2. Evolution of the helicity ratio $f_h = k\langle \boldsymbol{A}\cdot\boldsymbol{B}\rangle/\langle B^2\rangle$ for the magnetic energy and helicity and of the helicity ratio $\langle \boldsymbol{U}\cdot\nabla\times\boldsymbol{U}\rangle/k\langle U^2\rangle$ for the kinetic energy and helicity (k = 1, 5, 8). (a) It should be noted that the helicity ratio f_h of the large-scale magnetic field (red thick line) is not 1 initially. Rather, it begins from a low value and converges to 1 as the system becomes saturated. (b) The helicity ratio f_h of the large-scale magnetic field converges to −1. The constantly saturated magnetic helicity ratio implies that k for the large-scale field is clearly 1, not $\sqrt{2}$. Moreover, the wavenumber does not depend on time with the normalized code data.

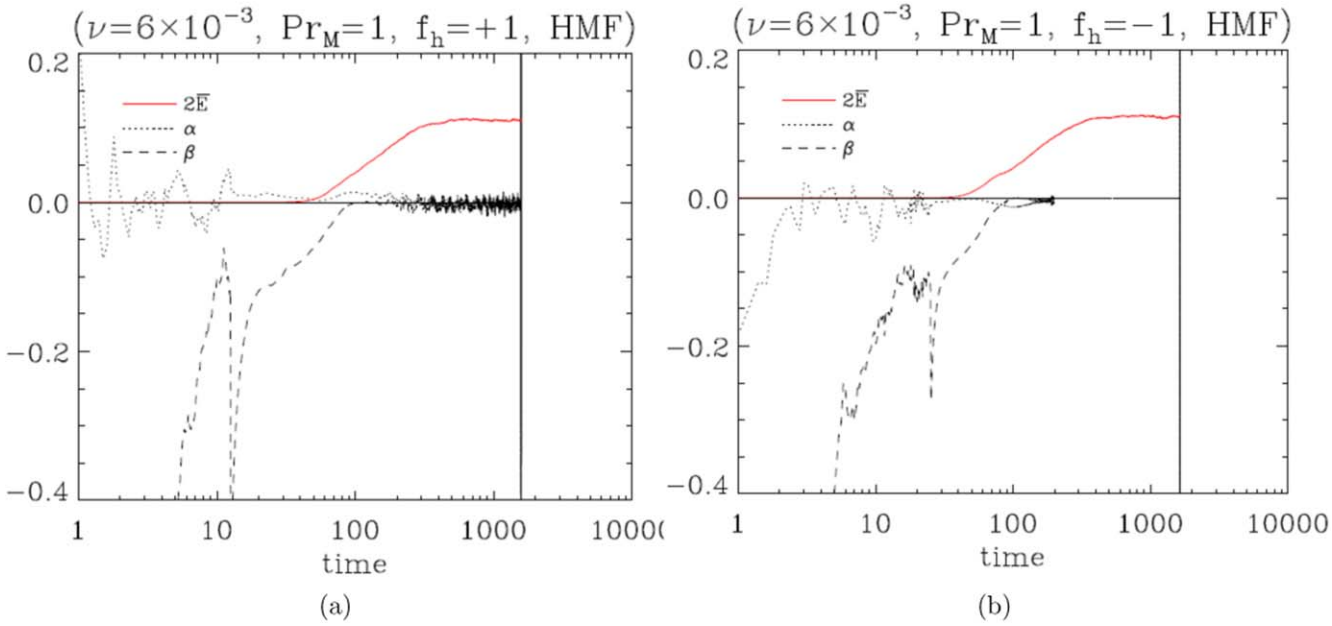

Figure 3. $\alpha(t)$, $\beta(t)$, and $\langle\overline{B}^2\rangle$ for $f_h = +1$ and $f_h = -1$. The small and early quenching of the α effect shows its limited effect on the growth of $2\overline{E}_M$. In contrast, the negative β has a positive effect with $\nabla^2(=-k^2)$. The average of 300 adjacent points are taken for $\alpha(t)$ and $\beta(t)$.

largest energy level with "$k = 5$" implies that the scale with this wavenumber is forced by an external energy source, which is consistent with our code setting. Unlike in HKFD, we see that the polarity of the large-scale magnetic helicity is consistent with that of the forcing helicity. That is, the polarizability of induced magnetic helicity in HMFD is the same as that of externally provided magnetic helicity. We will discuss the physical reason in Section 4.4.1.

Figure 3 includes the temporally evolving α and β effects and the large-scale magnetic energy $2\overline{E}_M$. The left (right) panel shows the evolution of $E_M$and the α and β effects for $f_h = 1$ ($f_h = -1$). The α effect for $f_h = 1$ positively oscillates and decreases significantly as E_M gets saturated. In contrast, the α effect for $f_h = -1$ negatively oscillates before it disappears. Theα effect is quenched much earlier than the slowly evolving E_M. The decreasing oscillation in both cases implies that α does not play a decisive role in the growth of the large-scale magnetic field except in the early time regime. Conversely, β retains the negative value in both cases and has a much larger size than α. This negative β, combined with the negative Laplacian $\nabla^2 \rightarrow -k^2$ in the Fourier space, can be considered as the actual source of the large-scale magnetic field. This is contradictory to the conventional dynamo theory, which concludes that β is always positive to diffuse magnetic energy. We will show that this conventional inference is valid only for the ideally isotropic system with reflection symmetry. When

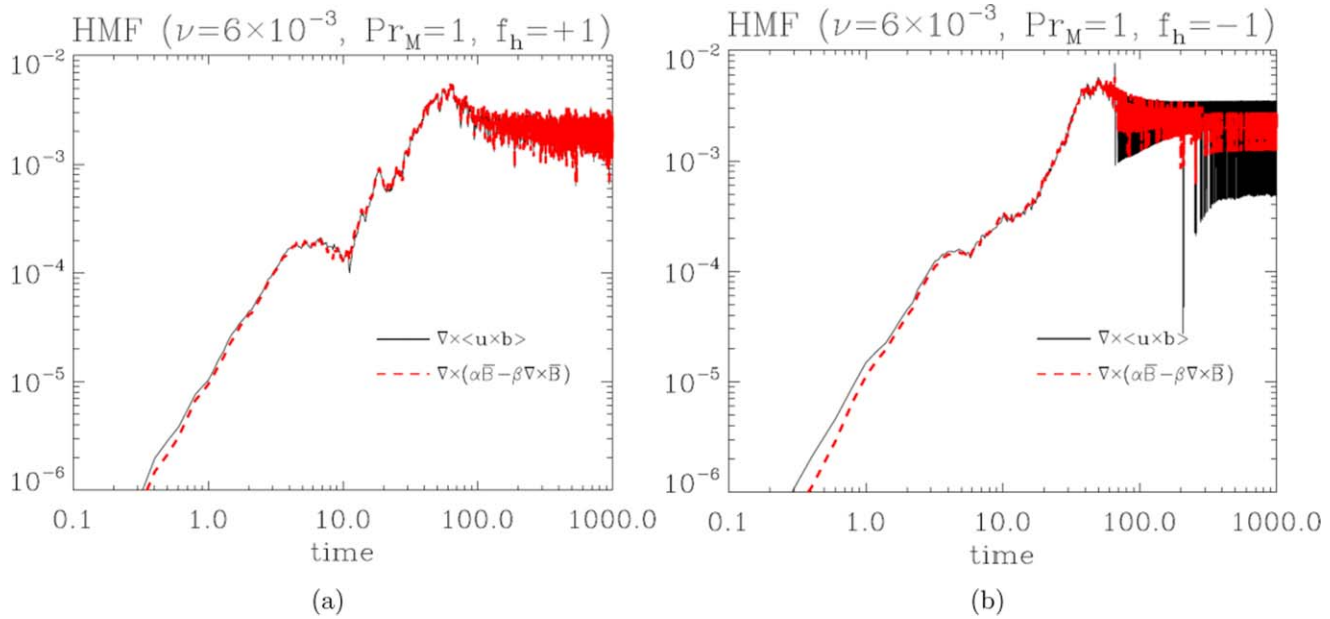

Figure 4. Comparison of $\nabla \times \langle \boldsymbol{u} \times \boldsymbol{b} \rangle$ with $\nabla \times (\alpha \bar{\boldsymbol{B}} - \beta \nabla \times \bar{\boldsymbol{B}})$.

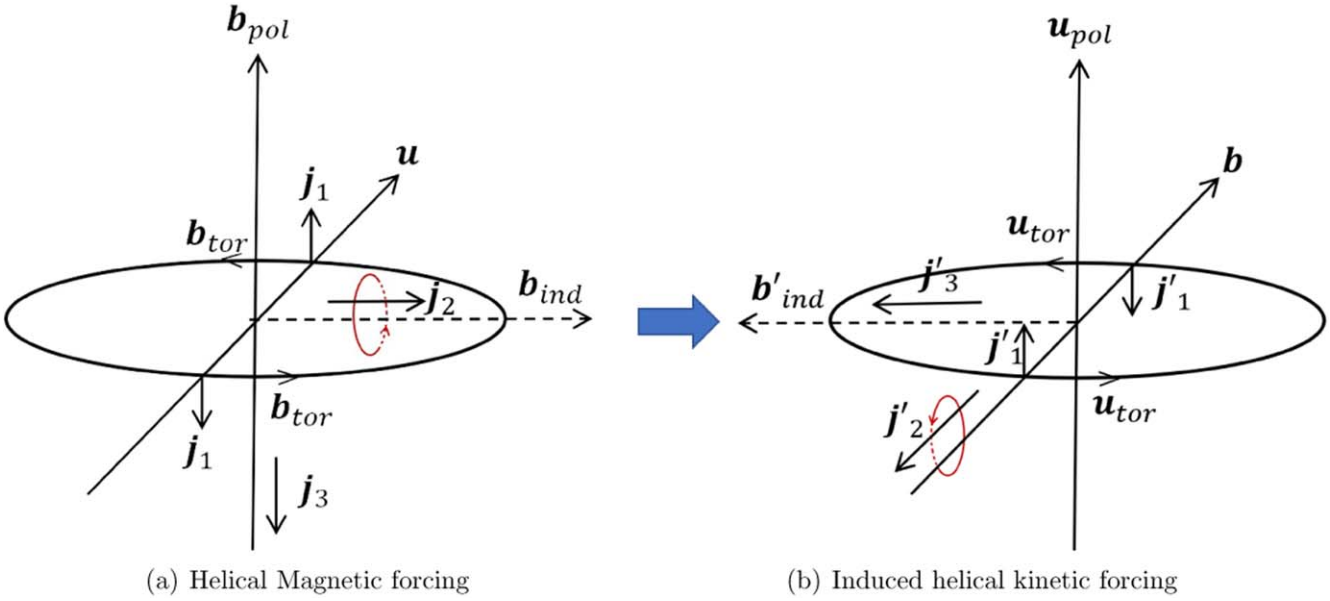

Figure 5. $\boldsymbol{j}_{1,\mathrm{up}}and\boldsymbol{j}_{1,\mathrm{down}}$ are represented as $\boldsymbol{j}_1$ for simplicity. (a) The right-handed (+) magnetic helicity yields $+|\boldsymbol{j}_2 \cdot \boldsymbol{b}_{\mathrm{ind}}|$, $-|\boldsymbol{j}_3 \cdot \boldsymbol{b}_{\mathrm{pol}}|$, and right-handed kinetic helicity $+|\boldsymbol{u}_{\mathrm{pol}} \cdot \nabla \times \boldsymbol{u}_{\mathrm{tor}}|$.

the symmetry is broken, "$\boldsymbol{u}$" in the small-scale regime can yield the antidiffusing effect of the magnetic field.

In Figure 4, we compared $\nabla \times \langle \boldsymbol{u} \times \boldsymbol{b} \rangle$ (black solid line) with $\nabla \times (\alpha \overline{\boldsymbol{B}} - \beta \nabla \times \overline{\boldsymbol{B}})$ (red dashed line) to verify Equations (6), (31), and (32). As mentioned, the exact range of the small-scale regime for EMF is unknown. Theoretically, the entire range for a wavenumber $k \geqslant 2$ in the Fourier space is supposed to be the small-scale regime, and that for $k = 1$ corresponds to the large-scale regime. However, if the entire range of $k \geqslant 2$ is considered to the turbulent EMF, the inferred growth rate exceeds the actual one, $\overline{\boldsymbol{B}}$. Therefore, we compared $\partial \overline{\boldsymbol{B}} / \partial t - \nu \nabla^2 \overline{\boldsymbol{B}}$ with $\nabla \times (\alpha \overline{\boldsymbol{B}} - \beta \nabla \times \overline{\boldsymbol{B}})$. The former uses only the simulation data for the large-scale magnetic energy data $(2\overline{E}_M)^{1/2}$. The latter requires the data of the large-scale magnetic helicity $\overline{H}_M$ in addition to $\overline{E}_M$. They are coincident in the transient mode ($t < \sim 100$ and in the range of $10^{-8} - 10^{-2}$). In the theoretical part, we analytically show that they are coincident. Note that Equations (31) and (32) are valid until the system becomes saturated, where $\overline{H}_M \sim 2\overline{E}_M$. As Figures 1, 2 show, $\overline{H}_M$ is different from $2\overline{E}_M$ in the transient state. As the field becomes saturated, $\overline{E}_M$ and $\overline{H}_M$ are so close that the logarithmic function diverges. For $f_h = -1$, we used absolute values for a clear comparison.

Figures 5, 6 show the field structure models. They are introduced to explain the dynamo process in an intuitive way. We discuss the mechanism in detail below.

Figure 7 is for the typical kinetic small-scale dynamo. The nonhelical random velocity field was driven at $k = 5$. The plot includes the large-scale kinetic energy E_V and magnetic energy E_M. Re_M is approximately 80. In comparison to LSD, E_M grows

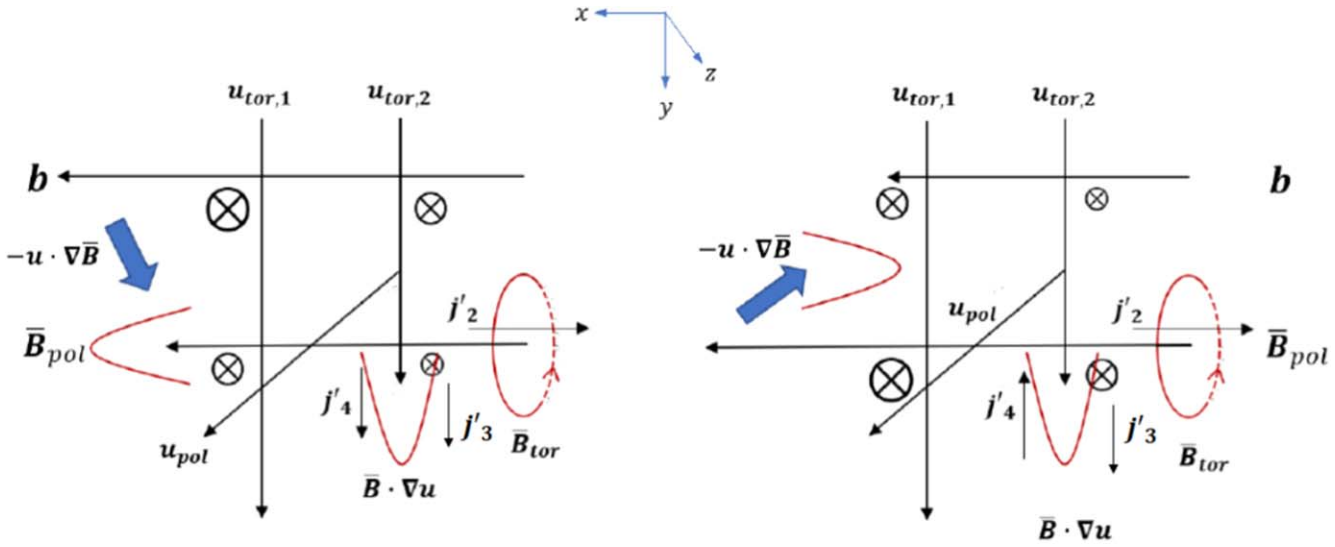

Figure 6. More detailed field structure based on EMF corresponding to Figure 5(b): $\nabla\times(\boldsymbol{U}\times\boldsymbol{B})=-\boldsymbol{U}\cdot\nabla\boldsymbol{B}+\boldsymbol{B}\cdot\nabla\boldsymbol{U}$. The left field structure is for the early time regime while $\bar{B}<b$. The right structure is for the magnetic back reaction with $\bar{B}\gtrsim b$ while $\bar{B}>b$. The symbol " $\otimes$ " marks the direction $(-\hat{z})$ of the induced current density $\boldsymbol{J}\sim\boldsymbol{U}\times\boldsymbol{B}$, and its size indicates the relative strength. $\boldsymbol{u}$ and $\boldsymbol{b}$ indicate the turbulent velocity and magnetic field, respectively. We use the symbol $\bar{\boldsymbol{B}}$ for the large-scale magnetic field. Conventionally, $\alpha\sim\boldsymbol{u}\times(\bar{\boldsymbol{B}}\cdot\nabla\boldsymbol{u})and\beta\sim\boldsymbol{u}\times(-\boldsymbol{u}\cdot\nabla\bar{\boldsymbol{B}})$ (omitting $\int d\tau$).

a little bit, and E_V is not quenched. Most magnetic energy is transferred to the small-scale regime, and its peak is located at $k\sim10$. These plots are to be compared with Figure 1(a), (b).

Figure 8 in the Appendix includes the evolving large-scale magnetic field from HKFD (a) and oscillating solar magnetic field (b). In Figure 8(a), Equations (3)–(6) were solved considering the positive kinetic helicity. In addition to the large-scale magnetic energy (solid line), the negative magnetic helicity (dashed line) also evolves and gets saturated. Although we did not include the evolving magnetic helicity in the small-scale regime, they positively (opposite to the sign of the large-scale magnetic helicity) evolve and become saturated faster than the large-scale helicity. In Figure 8(b), the contour plot of the solar net magnetic field is shown. The horizontal axis indicates the time, and the vertical one shows the latitude (northern–southern hemisphere) in the Sun. The different colors are for the opposite phases of the magnetic field. The converted timescale of amplification–annihilation–reverse is 22 yr. This is the result of Equations (23) and (24), which are converted Equation (22) in polar coordinates. This example is prepared to show how the α and β effects due to the Coriolis force and turbulence in the solar convection region $(0.7R_\odot<r<R_\odot)$ are applied to the solar magnetic field.

Figure 8 in the Appendix shows the time evolving $1/3\langle u^2\rangle$ and $1/6\langle\boldsymbol{u}\cdot\nabla\times\boldsymbol{u}\rangle$. This plot is to ensure that the overall β effect in HMFD can be negative.

Figure 9 in the Appendix shows the effect of the helical velocity field on magnetic diffusivity. Fully helical kinetic forcing is turned off at $t\sim200$ followed by nonhelical kinetic forcing, where $\langle\boldsymbol{u}\cdot\nabla\times\boldsymbol{u}\rangle=0$. After $t\sim200$, turbulent magnetic diffusivity becomes positive, which diffuses the magnetic field in the system. The result shows that β diffusion is negative with helicity and becomes positive without helicity. It should be kept in mind that we initially forced the system with a Gaussian helical turbulent energy. This is to realize the turbulent system without consideration of the forcing method. It is easy to separate the effect of magnetic helicity from other various influences. We will discuss the mechanism in the analytic section.

4. Discussions on Theoretical Analysis

We first introduce the derivation of α and β based on the conventional dynamo theory. We then suggest an alternative practical method to find them from the magnetic energy and helicity. Finally, we discuss the physical meaning of α and β using the field structure model, which is based on electrodynamics.

4.1. Conventional α and β

In the helical dynamo, small-scale EMF $\langle\boldsymbol{u}\times\boldsymbol{b}\rangle$ can be replaced with $\alpha\bar{\boldsymbol{B}}-\beta\nabla\times\bar{\boldsymbol{B}}$. This relation is approximately derived using a function iterative method with some appropriate closure theories such as MFT (Park & Blackman 2012a, 2012b), DIA (Yoshizawa 2011), and EDQNM (Pouquet et al. 1976).

In MFT, $\boldsymbol{u}$ and $\boldsymbol{b}$ are modified as (Maron & Blackman 2002; Biskamp 2008),

$$\boldsymbol{u}\times\boldsymbol{b}=\int^t\frac{\partial\boldsymbol{u}}{\partial\tau}d\tau\times\boldsymbol{b}+\boldsymbol{u}\times\int^t\frac{\partial\boldsymbol{b}}{\partial\tau}\,d\tau, \tag{10}$$

$$\sim\int^t\bar{\boldsymbol{B}}\cdot\nabla\boldsymbol{b}\,d\tau\times\boldsymbol{b}+\boldsymbol{u}\times\int^t(-\boldsymbol{u}\cdot\nabla\bar{\boldsymbol{B}}+\bar{\boldsymbol{B}}\cdot\nabla\boldsymbol{u})d\tau, \tag{11}$$

$$\sim\epsilon_{ijk}\int^t\bar{B}_l\nabla_l b_j\,d\tau\;b_k+\epsilon_{ijk}u_j\int^t(-u_l\nabla_l\bar{B}_k+\bar{B}_l\nabla_l u_k)d\tau. \tag{12}$$

We are looking for ith component of $\bar{\boldsymbol{B}}$ in the isotropic system without losing generality. Using $\langle x_k\partial_i x_j-x_j\partial_i x_k\rangle=1/3\langle\boldsymbol{x}\cdot\nabla\times\boldsymbol{x}\rangle$ and $\langle u_j\,u_l\rangle=1/3\langle u^2\rangle$, we get

$$\langle\boldsymbol{u}\times\boldsymbol{b}\rangle\sim\alpha\bar{\boldsymbol{B}}-\beta\nabla\times\bar{\boldsymbol{B}}, \tag{13}$$

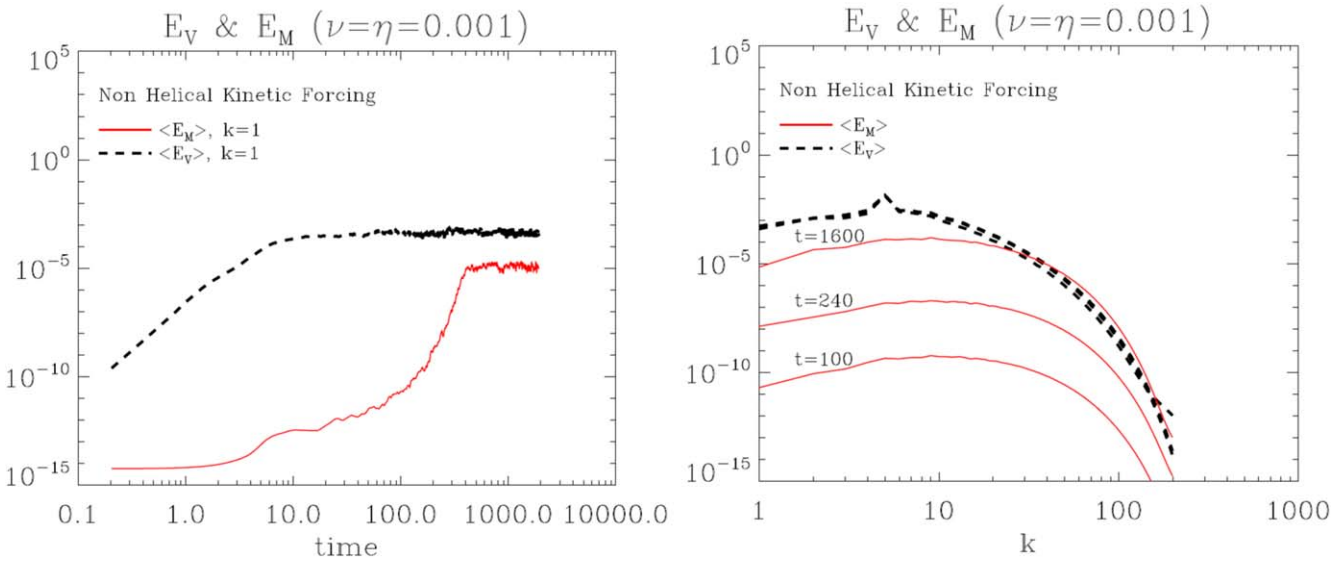

Figure 7. Nonhelical kinetic forcing small-scale dynamo. The nonhelical velocity field was given to $k = 5$. $\eta = \nu = 0.001$, and the magnetic Reynolds number Re_M is ~80. The left panel shows the temporal evolution of E_V and E_M. The right panel shows their spectra at $t = 100$, 240, 1600. The peak of E_M is located between the forcing scale and dissipation scale.

where

$$\alpha = \frac{1}{3}\int^t (\langle \boldsymbol{j}\cdot\boldsymbol{b}\rangle - \langle \boldsymbol{u}\cdot\nabla\times\boldsymbol{u}\rangle)d\tau, \tag{14}$$

$$\beta = \frac{1}{3}\int^t \langle u^2\rangle d\tau. \tag{15}$$

During the analytic calculation, a couple of turbulent variables with the triple correlation or higher-order terms are derived. They are dropped with the Reynolds rule or simply ignored under the assumption of being small. This may cause the increasing discrepancy between the real system and MFT as Re_M grows.

In DIA, the first step to finding α and β is similar to that of MFT, but instead of dropping the higher-order nonlinear terms, their effects are included in the formal Green function G. Then, the second-order moment is replaced by the statistical second-order relation as follows.

$$\langle X_i(k)X_j(-k)\rangle = (\delta_{ij} - \frac{k_ik_j}{k^2})E_X(k) + \frac{i}{2}\frac{k_l}{k^2}\epsilon_{ijl}H_X(k), \tag{16}$$

$$\left(\langle X^2\rangle = 2\int E_X(k)dk,\ \langle \boldsymbol{X}\cdot\nabla\times\boldsymbol{X}\rangle = \int H_X(k)dk\right).$$

Then, α and β are

$$\alpha = \frac{1}{3}\int d\boldsymbol{k}\int^t (G_M\langle \boldsymbol{j}\cdot\boldsymbol{b}\rangle - G_K\langle \boldsymbol{u}\cdot\nabla\times\boldsymbol{u}\rangle)d\tau, \tag{17}$$

$$\beta = \frac{1}{3}\int d\boldsymbol{k}\int^t (G_K\langle u^2\rangle + G_M\langle b^2\rangle)d\tau. \tag{18}$$

In DIA, the cross helicity $\langle \boldsymbol{u}\cdot\boldsymbol{b}\rangle$ is included and plays a role in EMF.

$$\gamma = \frac{1}{3}\int d\boldsymbol{k}\int^t (G_M + G_K)\langle \boldsymbol{u}\cdot\boldsymbol{b}\rangle d\tau. \tag{19}$$

The results are quite similar to those of MFT except for G_K and G_M and theγ tensor for cross helicity. The representation of theα coefficient implies its quenching as $G_M\langle \boldsymbol{j}\cdot\boldsymbol{b}\rangle$ approaches $G_K\langle \boldsymbol{u}\cdot\nabla\times\boldsymbol{u}\rangle$. However, the β effect depends on "$\langle u^2\rangle$" and "$\langle b^2\rangle$," which is distinct from other dynamo theories. As DIA considers both the kinetic approach and counter-kinetic (magnetically dominant) approach with Equation (16), the dependence on the turbulent magnetic energy is inevitable. DIA is statistically complete, but the practical way to calculate the Green function G is still unknown.

Another issue in MFT is the effect of the large-scale plasma motion $\overline{\boldsymbol{U}}$. If $\boldsymbol{U}\times\boldsymbol{B}$ is averaged over the large scale and applied with the Reynolds rule, two terms remain: $\xi \sim \overline{\boldsymbol{U}}\times\overline{\boldsymbol{B}} + \langle \boldsymbol{u}\times\boldsymbol{b}\rangle$, where $\overline{\boldsymbol{U}}\times\overline{\boldsymbol{B}}$ is usually excluded in a Galilean transformation. However, $\overline{\boldsymbol{U}}$ in simulation and observation does not disappear. Actually, the large-scale fluid motion is replaced with the radius r and angular velocity Ω near the tachocline ($\sim 0.7R_\odot$) in the solar convection regime.

In addition to MFT and DIA, α and β calculated with the EDQNM approximation show more or less similar physical properties, such as quenching of α and energy dependent of β (Pouquet et al. 1976).

$$\alpha = \frac{2}{3}\int^\infty \Theta_{kpq}(t)(\langle \boldsymbol{j}\cdot\boldsymbol{b}\rangle - \langle \boldsymbol{u}\cdot\nabla\times\boldsymbol{u}\rangle)dq, \tag{20}$$

$$\beta = \frac{2}{3}\int^\infty \Theta_{kpq}(t)\langle u^2\rangle\, dq. \tag{21}$$

Here, the triad relaxation time Θ_{kpq} is defined as $(1 - \exp(-\mu_{kpq}t))/\mu_{kpq}$, and the eddy damping operator μ_{kpq} is exactly found with the direct experiment. However, note that $\Theta \sim \mu_{kpq}^{-1}$, $\mu_{kpq} = \text{const.}$ as $t \to \infty$ for the stable system. Moreover, compared to α and β from MFT or DIA, these coefficients from EDQNM are 2 times larger. This is due to the second (one more) derivative over time leading to the fourth-order moment. When quasi-normalization is applied to the nonlinear moment, more energy and helicity terms are generated. Theoretically, this effect is modified with Θ_{kpq} and μ_{kpq}. In this paper, we will not show how to derive α and β further using EDQNM. Those who are interested in the detailed method can refer to the articles of Pouquet et al. (1976),

McComb (1990), Park & Cheoun (2022), and references therein.

Besides, the exact scale regime for EMF $\langle \boldsymbol{u} \times \boldsymbol{b} \rangle$ used in MFT, DIA, and EDQNM is not well defined. It is simply inferred from $\boldsymbol{X} - \overline{\boldsymbol{X}}$, which is supposed to be in the range of $k \geqslant 2$ in the Fourier space. However, the range participating in the amplification of the large-scale field is much narrower. Our previous work to find α and β with the conventional MFT shows that $\boldsymbol{u}$ and $\boldsymbol{b}$ (or α and β) exist only around the forcing scale (Figure 1 in Park & Blackman 2012b; Figure 1(b) in Park 2017). Kolmogorov's inertia range seems to separate the range of $\boldsymbol{u}$ and $\boldsymbol{b}$ for α and β from other scales. However, its exact range also depends on the various physical environments.

Nonetheless, despite all the limitations discussed above, Equation (8) itself is statistically correct and valid.

$$\frac{\partial \overline{\boldsymbol{B}}}{\partial t} \sim \nabla \times (\alpha \overline{\boldsymbol{B}} - (\beta + \eta) \nabla \times \overline{\boldsymbol{B}}). \tag{22}$$

This equation means that the $\boldsymbol{B}$ field is induced by the current density $\overline{\boldsymbol{J}} = \nabla \times \overline{\boldsymbol{B}}$ ($\sim \alpha$). At the same time, it grows or decays through diffusion $-\nabla \times \nabla \times \overline{\boldsymbol{B}} = \nabla^2 \overline{\boldsymbol{B}}$. The former shows the electromagnetic properties, and the latter shows the fluidic properties in magnetized plasma.

Equation (22) is not just formalistic. It can be applied to the practical solar dynamo. Equation (22) is divided into the poloidal part and toroidal one as follows (Charbonneau 2014):

$$\frac{\partial \overline{A}}{\partial t} = (\eta + \beta)\left(\nabla^2 - \frac{1}{\varpi^2}\right)\overline{A} - \frac{\boldsymbol{u}_p}{\varpi} \cdot \nabla(\varpi \overline{A}) + \alpha \overline{B}_{\rm tor}, \tag{23}$$

$$\frac{\partial \overline{B}_{\rm tor}}{\partial t} = (\eta + \beta)\left(\nabla^2 - \frac{1}{\varpi^2}\right)\overline{B}_{\rm tor} + \frac{1}{\varpi}\frac{\partial(\varpi \overline{B}_{\rm tor})}{\partial r}\frac{\partial(\eta + \beta)}{\partial r} - \varpi \boldsymbol{u}_p \cdot \nabla\left(\frac{\overline{B}_{\rm tor}}{\varpi}\right) - \overline{B}_{\rm tor} \nabla \cdot \boldsymbol{u}_p + \varpi(\nabla \times (\overline{A}\,\hat{e}_\phi)) \cdot \nabla \boldsymbol{\Omega} + \nabla \times (\alpha \nabla \times (\overline{A}\,\hat{e}_\phi)). \tag{24}$$

(Here, $\overline{\boldsymbol{B}}_{\rm pol} = \nabla \times \overline{\boldsymbol{A}}$, $\varpi = r \sin\theta$, and Ω is the angular velocity from convective motion $\overline{\boldsymbol{U}} = \boldsymbol{r} \times \boldsymbol{\Omega}$.)

The large-scale magnetic field (energy, helicity) and solar toroidal and toroidal magnetic fields are prepared in Figure 8 in the Appendix. The field profile in the left panel is the result of DNS solving Equations (3)–(6), forced with the positive kinetic helicity. If the polarity of α is negative, only the sign of the magnetic helicity turns over. The right panel includes the contour plot of the solar magnetic field from Equations (23) and (24). The polarization of α changes from positive to negative along with the solar latitude. The amplitude of α was carefully chosen to yield the least growing magnetic field affected by the tidal effects from nearby planets. These effects yield the periodic solar magnetic fields: amplification–annihilation–reverse in 22 yr.

4.2. Semi-analytic and Numerical Method

Now, we derive the semi-analytic definition of α and β. They are derived with the evolving equations of the large-scale magnetic energy and magnetic helicity deduced from Equation (8). We get

$$\begin{aligned} \overline{\boldsymbol{B}} \cdot \frac{\partial \overline{\boldsymbol{B}}}{\partial t} &= \alpha \overline{\boldsymbol{B}} \cdot \nabla \times \overline{\boldsymbol{B}} + (\beta + \eta)\overline{\boldsymbol{B}} \cdot \nabla^2 \overline{\boldsymbol{B}} \\ &= \alpha \overline{\boldsymbol{J}} \cdot \overline{\boldsymbol{B}} - (\beta + \eta)\overline{\boldsymbol{B}} \cdot \overline{\boldsymbol{B}}\,(k = 1) \\ \rightarrow \frac{\partial}{\partial t}\overline{E}_M &= -2(\beta + \eta)\overline{E}_M + \alpha \overline{H}_M. \end{aligned} \tag{25}$$

We can also derive the evolving magnetic helicity as follows.

$$\rightarrow \frac{d}{dt}\overline{H}_M = 4\alpha \overline{E}_M - 2(\beta + \eta)\overline{H}_M. \tag{26}$$

These two equations are functions of actual data $\overline{E}_M$and$\overline{H}_M$ resulting from all internal and external effects. A simple method to solve this coupled equation set is to diagonalize the matrix using a coefficient matrix P, which satisfies $[\overline{H}_M, \overline{E}_M] \equiv P\,[X, Y]$. The modified equation is represented as

$$\begin{bmatrix} \partial X/\partial t \\ \partial Y/\partial t \end{bmatrix} = P^{-1}\begin{bmatrix} -2(\beta + \eta) & 4\alpha \\ \alpha & -2(\beta + \eta) \end{bmatrix} \times P\begin{bmatrix} X \\ Y \end{bmatrix} = \begin{bmatrix} \lambda_1 & 0 \\ 0 & \lambda_2 \end{bmatrix}\begin{bmatrix} X \\ Y \end{bmatrix}. \tag{27}$$

The eigenvalues $\lambda_{1,2}$ can be found with the usual determinant condition for the nontrivial eigenvalue and eigenvector $(2(\beta + \eta) + \lambda)^2 - 4\alpha^2 = 0$. Then, we obtain eigenvalues and eigenvectors as follows. $\lambda_{1,2} = \pm 2\alpha - 2(\beta + \eta)$ and $P = \frac{1}{\sqrt{5}}\begin{bmatrix} 2 & 2 \\ 1 & -1 \end{bmatrix}$. The intermediate solution is

$$\begin{bmatrix} \overline{H}_M(t) \\ \overline{E}_M(t) \end{bmatrix} = \frac{1}{\sqrt{5}}\begin{bmatrix} 2X_0 e^{\int \lambda_1 d\tau} + 2Y_0 e^{\int \lambda_2 d\tau} \\ X_0 e^{\int \lambda_1 d\tau} - Y_0 e^{\int \lambda_2 d\tau} \end{bmatrix}, \tag{28}$$

where X_0 and Y_0 can be represented by H_0 and E_0. Finally, we get

$$2\overline{H}_M(t_n) = (2\overline{E}_M(t_{n-1}) + \overline{H}_M(t_{n-1}))e^{2\int_0^{t_n}(\alpha - \beta - \eta)d\tau} - (2\overline{E}_M(t_{n-1}) - \overline{H}_M(t_{n-1}))e^{2\int_0^{t_n}(-\alpha - \beta - \eta)d\tau}, \tag{29}$$

$$4\overline{E}_M(t_n) = (2\overline{E}_M(t_{n-1}) + \overline{H}_M(t_{n-1}))e^{2\int_0^{t_n}(\alpha - \beta - \eta)d\tau} + (2\overline{E}_M(t_{n-1}) - \overline{H}_M(t_{n-1}))e^{2\int_0^{t_n}(-\alpha - \beta - \eta)d\tau}. \tag{30}$$

$\overline{H}_M$ is always smaller than $2\overline{E}_M$, which satisfies the realizability condition. However, $\overline{H}_M \rightarrow 2\overline{E}_M$ as the system becomes saturated. In the case of a right-handed HMFD, clearly $\alpha > 0$ so that the first terms in Equations (29) and (30) are dominant. This means that $\overline{H}_M(t_n)$ and $\overline{E}_M(t_n)$ are positive. In the case of a left-handed HMFD, the second term is dominant. This indicates that $\overline{H}_M(t_n)$ is negative, but $\overline{E}_M(t_n)$ is positive. On the contrary, in the case of a positively forced HKFD, α is negative so that the second term in each equation is dominant leading to negative $\overline{H}_M$. Still, $\overline{E}_M$ is not influenced by the chirality of forcing. These inferences are consistent with the simulation result of HKFD or HMFD. α and β can be obtained from the above results or Equations (25) and (26) (Park 2020):

$$\alpha(t) = \frac{1}{4}\frac{d}{dt}\log_e\left|\frac{2\overline{E}_M(t) + \overline{H}_M(t)}{2\overline{E}_M(t) - \overline{H}_M(t)}\right|, \tag{31}$$

$$\beta(t) = -\frac{1}{4}\frac{d}{dt}\log_e |(2\overline{E}_M(t) - \overline{H}_M(t))(2\overline{E}_M(t) + \overline{H}_M(t)| - \eta. \quad (32)$$

For the temporally evolving profiles, we need the data for $\overline{E}_M(t)$,$\overline{H}_M(t)$,$\partial\overline{E}_M/\partial t$, and $\partial\overline{H}_M/\partial t$ in each time step "t_n." In Figure 3, we used the data for $\overline{E}_M(t)$and$\overline{H}_M(t)$ from simulation (DNS) solving Equations (3)–(6) instead of Equation (8). As the wavenumber in the Fourier space is inversely proportional to the eddy scale $k \sim 1/\ l$, E_M and H_M for $k = 1$ correspond to the large-scale data. Further, $\partial\overline{E}_M/\partial t$ (or $\partial\overline{H}_M/\partial t$) can be approximately obtained from $\Delta\overline{E}_M/\Delta t \sim (\overline{E}_M(t_n) - \overline{E}_M(t_{n-1}))/(t_n - t_{n-1})$. Additionally, these results are verified in Figure 4(a), (b). Both plots compare $\nabla \times \langle \boldsymbol{u} \times \boldsymbol{b} \rangle$ with $\nabla \times (\alpha\overline{\boldsymbol{B}} - \beta\nabla \times \overline{\boldsymbol{B}})$.

Analytically, we expand Equations (31) and (32) with the assumption of fully helical fields ($2\overline{E}_M \sim \overline{H}_M$ or $\nabla \times \overline{A} = \overline{A}$).

$$\alpha - \beta - \eta = \frac{1}{2}\frac{\partial}{\partial t}\log_e|2\overline{E}_M + \overline{H}_M| = \frac{1}{2(2\overline{E}_M + \overline{H}_M)}\left(2\frac{\partial\overline{E}_M}{\partial t} + \frac{\partial\overline{H}_M}{\partial t}\right) \simeq \frac{1}{\overline{B}}\frac{\partial\overline{B}}{\partial t}. \quad (33)$$

We apply this result to the equation for the large-scale magnetic field,

$$\frac{\partial\overline{\boldsymbol{B}}}{\partial t} = \alpha\nabla \times \overline{B} - \beta\nabla \times \nabla \times \overline{\boldsymbol{B}} + \eta\nabla^2\overline{\boldsymbol{B}} \simeq (\alpha - \beta - \eta)\overline{\boldsymbol{B}} \sim \frac{\partial\overline{\boldsymbol{B}}}{\partial t}. \quad (34)$$

4.3. Derivation of β

The negative β can be derived with the field structure model with a tensor identity. However, here we derive a more general result with a statistical identity for the second-order moment. The β effect is derived from $\langle \boldsymbol{u} \times (-\boldsymbol{u} \cdot \nabla\overline{\boldsymbol{B}})\rangle = \langle -\epsilon_{ijk}u_j(r)u_m(r+l)\partial\overline{B}_k/\partial\overline{r}_m\rangle \sim \beta(-\nabla \times \overline{\boldsymbol{B}})$. In conventional theory, the turbulent moment $\langle u_j(r)u_m(r+l)\rangle$ is simply replaced by $1/3\langle u^2\rangle\delta_{jm}$ with $l \to 0$. The trace of the 3×3 tensor $\langle u_j u_m\rangle$ becomes energy density and is always positive leading to a positive β effect. The intuitive assumption may be valid in hydrodynamics. However, in MHD it is too simplified. In particular, when the field is helical, the off diagonal terms in the tensor are not negligible. A more general representation for the second-order moment is to be used (McComb 1990; Lesieur 2008)

$$U_{jm} \equiv \langle u_j(r)u_m(r+l)\rangle = A(l)\delta_{jm} + B(l)l_j l_m + C(l)\epsilon_{jms}l_s. \quad (35)$$

In the reference frame of $\vec{l} = (l, 0, 0)$ or any other appropriate coordinates, we can easily infer the relation of "A," "B," and "C" as follows: $U_{11} = A + l^2B \equiv F$, $U_{22} = A \equiv G$, $U_{12} = lC \equiv H$. These results can be applied to any homogeneous and isotropic system without loss of generality. Equation (35) is

$$U_{jm} = G\ \delta_{jm} + \frac{(F-G)}{l^2}\ l_j l_m + H\epsilon_{jms}\frac{l_s}{l}. \quad (36)$$

Under the incompressibility condition $\nabla \cdot \boldsymbol{U} = 0$, we get an additional constraint of $G = F + (l/2)\partial F/\partial l$.

$$U_{jm} = \left(F + \frac{l}{2}\frac{\partial F}{\partial l}\right)\delta_{jm} - \frac{l}{2l^2}\frac{\partial F}{\partial l}l_j l_m + H\epsilon_{jms}\frac{l_s}{l}. \quad (37)$$

Now, we apply this general result to our β derivation. If $j = m$, only the first term F remains, which can be defined as $u^2/3(= E_V/6)$. If $j \neq m$, the first and second terms disappear; however, in general the third term cannot be dropped. However, as the relation $\langle\epsilon_{ijk}u_j(r)u_m(r+l)\partial\overline{B}_k/\partial\overline{r}_m\rangle \to -\langle\epsilon_{ijk}l_j l_m/2l\ \partial F/\partial l\rangle\partial\overline{B}_k/\partial\overline{r}_m$ implies that any possible "m" makes the average *zero*, it can be also neglected. For the physical meaning of H, we need to use the definition of helicity (Lesieur 2008).

$$\begin{aligned} H_V &= \lim_{y \to x}\langle \boldsymbol{u}(x) \cdot \nabla \times \boldsymbol{u}(y)\rangle \\ &= \lim_{y \to x}\epsilon_{ijn}\left\langle u_i\frac{\partial u_n}{\partial y_j}\right\rangle \\ &= \lim_{l \to 0}\epsilon_{ijn}\frac{\partial U_{in}(l)}{\partial l_j}\ (\leftarrow y = x + l) \\ &= \lim_{l \to 0}\epsilon_{ijn}\epsilon_{ins}\frac{\partial}{\partial l_j}\left(H\frac{l_s}{l}\right) \\ &= \lim_{l \to 0}\epsilon_{ijn}\epsilon_{ins}\left(\delta_{js}\frac{H}{l} - \frac{l_j l_s}{l^3}H + \frac{l_j l_s}{l^2}\frac{\partial H}{\partial l}\right) \\ &= -\frac{6}{l}H. \end{aligned} \quad (38)$$

In the last step, we used $\epsilon_{ijn}\epsilon_{ins} = -2\delta_{js}$ and $\partial H/\partial l \to H/l$ with $l \to 0$. Then, Equation (37) is[4]

$$U_{jm} = \frac{\langle u^2\rangle}{3}\delta_{jm} - \epsilon_{jms}\frac{l_s}{6}H_V. \quad (39)$$

Finally, we can simplify the tensor representation as

$$\left\langle -\epsilon_{ijk}u_j(r)u_m(r+l)\frac{\partial\overline{B}_k}{\partial\overline{r}_m}\right\rangle = -\frac{1}{3}\langle u^2\rangle\epsilon_{ijk}\frac{\partial\overline{B}_k}{\partial\overline{r}_m}\delta_{jm} + \epsilon_{ijk}\epsilon_{jms}\frac{l_s}{6}H_V\frac{\partial\overline{B}_k}{\partial\overline{r}_m}. \quad (40)$$

The first term in RHS is clearly found to be $\sim(\nabla \times \overline{\boldsymbol{B}})_i$. For the second one, we refer to the vector identity $\epsilon_{ijk}\epsilon_{jms} = \delta_{km}\delta_{is} - \delta_{ks}\delta_{im}$. This relation shows the condition in the nontrivial case. We use $m \to i$ and $s \to k$, and other information remain implicit. We take the average over the large scale and separate the scale regimes. Then, we can rewrite the second term as follows:

$$\left\langle \epsilon_{ijk}\epsilon_{jms}\frac{l_s}{6}H_V\frac{\partial\overline{B}_k}{\partial\overline{r}_m}\right\rangle \to \langle\epsilon_{jik}\frac{l}{6}H_V\rangle\ \epsilon_{ijk} \times \frac{\partial\overline{B}_k}{\partial\overline{r}_i} \to \frac{l}{6}H_V(\nabla \times \overline{\boldsymbol{B}})_j. \quad (41)$$

[4] Note that $lH_V \neq 0$ as $l \to 0$. It should be $lH_V \to f(l)\epsilon_{ijk}\langle u_i u_k\rangle$, where the nontrivial $f(l)$ is from the dimensional analysis of $[l/\partial]$. In principle, we can apply it to Equation (40) again, but we derive the equation as usual in the turbulence theory.

Note that we used the normal permutation rule and regarded l_s as a small constant that belongs to the small-scale regime. Finally,

$$\left(\frac{1}{3}\langle u^2\rangle - \frac{l}{6}H_V\right)(-\nabla \times \overline{\boldsymbol{B}}). \tag{42}$$

The series of these analysis is based on the general turbulence theory. It is not limited to some specific forcing flow, and neither is Equations (31) and (32).

We infer the constraint of "l":

$$\langle u(r)u(r+l)\rangle \equiv \langle u^2(r)\rangle g(r) \sim \frac{1}{3}\langle u^2\rangle - \frac{l}{6}\langle \boldsymbol{u}\cdot\nabla\times\boldsymbol{u}\rangle \sim \frac{(2-lk)}{6}\langle u^2\rangle. \tag{43}$$

The condition of $2-lk<0$ is actually the correlation position that makes $g(r)$ negative, which is a typical property of parallel correlation functions (Davidson 2004). As k for the small scale is larger than 2, the condition of a negative β is not a hard one. Figure 8 in the Appendix shows how $1/3\langle u^2\rangle$ and $1/6\ \langle \boldsymbol{u}\cdot\nabla\times\boldsymbol{u}\rangle$ evolve. It is easy to note that $\langle \boldsymbol{u}\cdot\nabla\times\boldsymbol{u}\rangle \sim k\langle u^2\rangle$ with $k=2, 3, 4, ...$ is larger than $\langle u^2\rangle$ both in the Fourier space and real space.

In principle, a spatial average "$\langle\ \rangle$" corresponds to the quantity measured at some instant position ($l=0$). However, this does not mean the exclusion of the effects of neighbor eddies. Diffusion itself means the exchange of energy and materials with other eddies, not itself. Moreover, "l" is a prerequisite quantity to explain the orientation (helicity) of two vectors (Lesieur 2008). So, we need the second term H_V with "l" as some small distance from other eddies for the complete description of turbulence. Actually, β shown in Figures 3, 4, 9(b) and derived from Equations (32) and (33) and the simulation data clearly shows the effect of H_V. These equations and DNS data are exact results.

In this section, we considered the effect of helicity in β, i.e., $\langle u(r)u(r+l)\rangle$. However, in principle, we can also expand the helical effect in α. However, the expansion of $\boldsymbol{u}$ or $\boldsymbol{b}$ in $\langle \boldsymbol{u}\cdot\nabla\times\boldsymbol{u}\rangle$ and $\langle \boldsymbol{b}\cdot\nabla\times\boldsymbol{b}\rangle$ leads to nonlinearly constrained higher-order terms, which are not clearly solved. This is why Kraichnan (1976) directly expanded the unknown α under the assumption of a strong helical field. Kraichnan derived the negative magnetic diffusion effect in Lagrangian formation in a formalistic and general way (see also Brandenburg & Sokoloff 2002). We introduce part of his result here but will not discuss the work in detail. The reader interested in their works can refer to the references.

$$\frac{\partial\overline{\boldsymbol{B}}}{\partial t} = \beta_0\nabla^2\overline{\boldsymbol{B}} + \tau_2\nabla\times\langle\alpha\nabla\times\alpha\rangle\,\overline{\boldsymbol{B}} \rightarrow (\beta_0 - \tau_2 A)\nabla^2\overline{\boldsymbol{B}}. \tag{44}$$

Here, $\beta_0 = \int^{\tau_1} u_0^2\,dt \sim \tau_1 u_0^2$, $\alpha(\boldsymbol{x}, t) = (-)1/3\langle \boldsymbol{u}\cdot\omega\rangle\tau_1$, $\langle\alpha(\boldsymbol{x}, t)\alpha(\boldsymbol{x}', t')\rangle = A(x-x')D_2(t-t')$, $\tau_2 = \int^{\infty} D_2(t)dt$. β_0 is the conventional positive magnetic diffusion effect. However, $-\tau_2 A$, which is from the correlation of $\langle\alpha\alpha\rangle$, actually plays the role of the negative magnetic diffusion β effect.

There are more theoretical and experimental works associated with the negative magnetic diffusivity (Lanotte et al. 1999 and references therein). They are based on an $\alpha-\alpha$ correlation in the strong helical system. Further, Giesecke et al. (2014) found that the turbulent magnetic diffusivity was negative. Although they argued that the net diffusivity ($\eta_{\rm turb}+\eta$) became positive again, what we focus on is the turbulent magnetic diffusivity $\eta_{\rm turb}$, not the molecule-originated η. The negative magnetic diffusivity was also observed in another liquid sodium experiment (Cabanes et al. 2014). They found that small-scale turbulent fluctuations ($\sim u$) contribute to negative magnetic diffusivity in the interior region. The α effect practically disappears for the lower Re_M value; instead, the β effect increases strongly and promotes the dynamo action.

In comparison with these specific conditions, Equations (31) and (32) are from the general Equation (22) and turbulence theory. The results produce the weak α and negative β with a randomly driven helical forcing DNS source (Equation (9)). All of these results strongly imply the role of magnetic diffusion in a plasma system.

The weak α effect compared to the β one is a very reasonable phenomenon in plasma or fluid systems. In vacuum or free space, the magnetic field propagates unlimitedly ($\sim \alpha J$). However, in a plasma system, the electromagnetic energy is coupled with massive charged particles to lose its energy. Growth and propagation mainly depend on diffusion ($\beta\nabla^2 \rightarrow -\beta k^2$).

So far, we have argued that the main reason of negative magnetic diffusivity is the helical component in "u." We can refer to the numerically supporting result in Figure 9 in the Appendix. When the helical kinetic forcing is turned off at $t\sim 200$ and nonhelical forcing is on, negative β becomes positive. This negative magnetic diffusivity suppresses the growth of a large-scale magnetic field.

4.4. Intuitive Investigation of Magnetic Field Amplification

4.4.1. α Effect

The right-handed helical magnetic structure in Figure 5(a) is composed of the toroidal magnetic component $\boldsymbol{b}_{\rm tor}$ and poloidal part $\boldsymbol{b}_{\rm pol}$. Statistically, $\boldsymbol{b}_{\rm tor}$ and $\boldsymbol{b}_{\rm pol}$ are not distinguished in a homogeneous and isotropic system. However, if we remove reflection symmetry from the system, $\boldsymbol{b}_{\rm tor}$ and $\boldsymbol{b}_{\rm pol}$ become independent components playing different roles with $\boldsymbol{u}$.

The interaction between $\boldsymbol{u}$ and $\boldsymbol{b}_{\rm tor}$ yields a current density, i.e., $\boldsymbol{u}\times\boldsymbol{b}_{\rm tor}\sim\boldsymbol{j}_{1,\rm down}$ and $\boldsymbol{j}_{1,\rm up}$ in the front and back. These two components induce a new magnetic field $\boldsymbol{b}_{\rm ind}$. At the same time, $\boldsymbol{u}\times\boldsymbol{b}_{\rm pol}$ generates $\boldsymbol{j}_2$. This current density forms the right-handed magnetic helicity with $\boldsymbol{b}_{\rm ind}$: $\langle \boldsymbol{j}_2\cdot\boldsymbol{b}_{\rm ind}\rangle \rightarrow k_2^2\langle \boldsymbol{a}_2\cdot\boldsymbol{b}_{\rm ind}\rangle$, which is a (pseudo) scalar to be added to the system. There is also a possibility that $\boldsymbol{u}$ and $\boldsymbol{b}_{\rm ind}$ induce $\boldsymbol{j}_3$ yielding a left-handed magnetic helicity $\langle \boldsymbol{j}_3\cdot\boldsymbol{b}_{\rm pol}\rangle$. However, the induced magnetic field from $\boldsymbol{j}_3$ is weakened by the externally provided $\boldsymbol{b}_{\rm tor}$.

On the other hand, $\boldsymbol{j}_1\times\boldsymbol{b}_{\rm tor}$ and $\boldsymbol{j}_2\times\boldsymbol{b}_{\rm pol}$ generate a Lorentz force toward $-\boldsymbol{u}$, which may look as a suppressing plasma motion. However, $\boldsymbol{j}_2\times\boldsymbol{b}_{\rm tor}$ at the right and left ends yields a rotation effect, which is toward "$-\boldsymbol{u}$." This rotation with those two interactions generates a right-handed kinetic helicity $\langle \boldsymbol{u}\cdot\nabla\times\boldsymbol{u}\rangle$. The interaction between the current density and magnetic field produces two effects. The magnetic pressure effect $-\nabla B^2/2$ from $\boldsymbol{j}_1\times\boldsymbol{b}_{\rm tor}$ and $\boldsymbol{j}_2\times\boldsymbol{b}_{\rm pol}$ suppresses the plasma motion with thermal pressure $-\nabla P$. $\boldsymbol{j}_2\times\boldsymbol{b}_{\rm tor}$ creates a rotational force to form kinetic helicity with the two suppressing effects. As the Fourier-transformed Lorentz force

$\boldsymbol{j}(p) \times \boldsymbol{b}(q) \sim \partial \boldsymbol{u}(k)/\partial t$ shows, wavenumbers "$\boldsymbol{p}$" and "$\boldsymbol{q}$" are constrained by the relation of $\boldsymbol{p} + \boldsymbol{q} = \boldsymbol{k}$.

The induced right-handed kinetic helicity in Figure 5(b) again generates $\boldsymbol{j}'_1$ with $\boldsymbol{b}$ in the front and back. The spatially inhomogeneous current density from $\boldsymbol{j}'_{1,\mathrm{up}}$ and $\boldsymbol{j}'_{1,\mathrm{down}}$ induces $\boldsymbol{b}'_{\mathrm{ind}}$ leading to $\boldsymbol{j}'_2$ with $\boldsymbol{u}_{\mathrm{pol}}$, i.e., $\boldsymbol{j}'_2 \sim \boldsymbol{u}_{\mathrm{pol}} \times \boldsymbol{b}'_{\mathrm{bind}}$. Then, $\boldsymbol{j}'_2$ forms a left-handed magnetic helicity with $\boldsymbol{b}$. Further, $\boldsymbol{u}_{\mathrm{pol}} \times \boldsymbol{b}$ yields $\boldsymbol{j}'_3$ leading to a right-handed magnetic helicity with $\boldsymbol{b}'_{\mathrm{ind}}$. The net helicity is inferred to be $-|\langle \boldsymbol{j}'_2 \cdot \boldsymbol{b}\rangle| + |\langle \boldsymbol{j}'_3 \cdot \boldsymbol{b}'_{\mathrm{ind}}\rangle|$. However, if $|\langle \boldsymbol{j}'_3 \cdot \boldsymbol{b}'_{\mathrm{ind}}\rangle|$ is the main process, $\boldsymbol{b}$ will decay in the resistive plasma system. Therefore, the main process in this structure is $-|\langle \boldsymbol{j}'_2 \cdot \boldsymbol{b}\rangle|$.

The summed up net current (magnetic) helicity is $|\langle \boldsymbol{j}_2 \cdot \boldsymbol{b}_{\mathrm{ind}}\rangle| - |\langle \boldsymbol{j}'_2 \cdot \boldsymbol{b}\rangle|$. It should be noted that the latter $-|\langle \boldsymbol{j}'_2 \cdot \boldsymbol{b}\rangle|$ is from $+|\langle \boldsymbol{b}_{\mathrm{pol}} \cdot \nabla \times \boldsymbol{b}_{\mathrm{tor}}\rangle|$. As this subsidiary grows, the overall current helicity decreases, which is the intuitive model for the oscillating α quenching. Briefly, $+|\langle \boldsymbol{b}_{\mathrm{pol}} \cdot \nabla \times \boldsymbol{b}_{\mathrm{tor}}\rangle| \underset{\text{Lorentz}}{\rightleftarrows} + |\langle \boldsymbol{u}_{\mathrm{pol}} \cdot \nabla \times \boldsymbol{u}_{\mathrm{tor}}\rangle| \underset{\alpha}{\rightleftarrows} -|\langle \boldsymbol{b}_{\mathrm{pol}} \cdot \nabla \times \boldsymbol{b}_{\mathrm{tor}}\rangle| \underset{\text{Lorentz}}{\rightleftarrows} - |\langle \boldsymbol{u}_{\mathrm{pol}} \cdot \nabla \times \boldsymbol{u}_{\mathrm{tor}}\rangle| \underset{\alpha}{\rightleftarrows} +|\langle \boldsymbol{b}_{\mathrm{pol}} \cdot \nabla \times \boldsymbol{b}_{\mathrm{tor}}\rangle| \rightarrow \ldots$

4.4.2. β Effect

Figure 6 presents a more detailed right-handed helical kinetic structure of Figure 5(b). It is based on the geometrical meaning of "$\nabla \times (\boldsymbol{u} \times \overline{\boldsymbol{B}}) \sim \overline{\boldsymbol{B}} \cdot \nabla \boldsymbol{u} - \boldsymbol{u} \cdot \nabla \overline{\boldsymbol{B}} > 0$" for the amplification of the magnetic field. Here, we named "$-\boldsymbol{u} \cdot \nabla \overline{\boldsymbol{B}}$" as the "local transfer (advective) term," and we call "$\overline{\boldsymbol{B}} \cdot \nabla \boldsymbol{u}$" the "nonlocal transfer term." The symbol "$\otimes$" marks the direction of the current density "$\boldsymbol{u}_{tor,i} \times (\boldsymbol{b}, \overline{\boldsymbol{B}}_{\mathrm{pol}}) \sim \boldsymbol{J}_i$" heading toward $-\hat{\boldsymbol{z}}$. The size of $\otimes$ indicates its relative strength. Its distribution is spatially inhomogeneous so that the nontrivial curl effect generates two magnetic fields: a locally transferred field $\int d\tau (-\boldsymbol{u} \cdot \nabla \overline{\boldsymbol{B}})\ \hat{\boldsymbol{x}}$ and a nonlocally transferred field $\int d\tau (\overline{\boldsymbol{B}} \cdot \nabla \boldsymbol{u})\ \hat{\boldsymbol{y}}$.

$\boldsymbol{j}'_3$ from $\boldsymbol{u}_{\mathrm{pol}} \times (\boldsymbol{b}$ or $\overline{\boldsymbol{B}}_{\mathrm{pol}})$ yields positive H_M with $\overline{\boldsymbol{B}} \cdot \nabla \boldsymbol{u}$ (without $\int d\tau$). Further, $\boldsymbol{u}_{\mathrm{pol}} \times \overline{\boldsymbol{B}} \cdot \nabla \boldsymbol{u}$ produces $\boldsymbol{j}'_2$ leading to negative H_M with $\overline{\boldsymbol{B}}$ (α effect). Moreover, while $\overline{\boldsymbol{B}}$ is weak, $\boldsymbol{u}_{\mathrm{pol}} \times (-\boldsymbol{u} \cdot \nabla \overline{\boldsymbol{B}})$ yields $+j'_4 \hat{y}$ producing positive H_M with $\overline{\boldsymbol{B}} \cdot \nabla \boldsymbol{u}$ (left panel). However, as $\overline{\boldsymbol{B}}$ grows due to the α effect, the direction of $(-\boldsymbol{u} \cdot \nabla \overline{\boldsymbol{B}})$ changes followed by $+j'_4 \hat{y} \rightarrow -j'_4 \hat{y}$. A negative H_M value is produced by $-j_4 \hat{y}$ and $\overline{\boldsymbol{B}} \cdot \nabla \boldsymbol{u}$, which has the same polarization as $-j_2 \hat{x}$ and $\overline{\boldsymbol{B}}$ (right panel). This is the physical meaning of a negative β in the field structure model (see $\beta \sim \langle \boldsymbol{u} \times \int^t -\boldsymbol{u} \cdot \nabla \overline{\boldsymbol{B}}\ d\tau \rangle$).

5. Summary

In this paper, we have discussed the negative magnetic diffusion in HMFD. HMFD has several features distinguishing it from a helical kinetic forcing dynamo (HKFD). Externally given E_M is converted into E_V through the Lorentz force, which activates the plasma motion followed by EMF. This nontrivial EMF transports E_M into the large- and small-scale region. E_V in HMFD is subsidiary to the migration of E_M so that magnetic Reynolds number $\mathrm{Re}_M (= UL/\eta)$ is negligibly small. This means that the energy dissipation due to plasma fluctuation is very small. The large-scale magnetic energy $\overline{E}_M$ is amplified and saturated more efficiently than that of HKFD. This may be able to explain the big gap between the cosmological seed magnetic field ($\sim 10^{-62} - 10^{-19} G$) and the galactic magnetic field ($\sim 10^{-6}$ G).

The nonlinear interaction between the helical field and plasma can be explained with the α and β effects, which linearize the nonlinear dynamo process. As the exact definitions of α and β are not yet known, we calculated them using Equations (31) and (32), which were derived from Equations (25) and (26). Compared to the conventional theory, α becomes negligible much earlier than the saturation of $\overline{\boldsymbol{B}}$. In contrast, β remains negative and becomes saturated along with $\overline{E}_M$. Clearly, the effect of α as a generator of $\overline{E}_M$ is limited. Rather, the negative β effect plays a substantial role in amplifying $\overline{E}_M$ with the Laplacian $\nabla^2 \rightarrow -k^2 (k = 1)$.

The main dynamo processes in the system are as follows: $\int \partial \boldsymbol{u}/\partial t\, d\tau \times \boldsymbol{b} \sim \int \overline{\boldsymbol{B}} \cdot \nabla \boldsymbol{b}\ d\tau \times \boldsymbol{b} \sim \int (\boldsymbol{b} \cdot \nabla \times \boldsymbol{b}) d\tau\ \overline{\boldsymbol{B}}$ (α_M, positive magnetic helicity), $\boldsymbol{u} \times \int \partial \boldsymbol{b}/\partial t\ d\tau \sim \boldsymbol{u} \times \int \overline{\boldsymbol{B}} \cdot \nabla \boldsymbol{u}\ d\tau \sim -\int (\boldsymbol{u} \cdot \nabla \times \boldsymbol{u}) d\tau\ \overline{\boldsymbol{B}}$ (α_V, negative magnetic helicity), $\boldsymbol{u} \times \int -\boldsymbol{u} \cdot \nabla \overline{\boldsymbol{B}}\ d\tau \sim \beta\, \nabla^2 \overline{\boldsymbol{B}}$ (positive magnetic helicity). The first two interactions correspond to α quenching, and the last one is associated to the negative β effect. These α and negative β effects commonly originate from the helical component in the velocity field. In addition to the helical effect in the conventional α effect, we newly showed that the role of the helical velocity field in the advection term $-\boldsymbol{u} \cdot \nabla \overline{\boldsymbol{B}}$ leads to the negative β effect.

We showed the evolution of α and β in Figure 3 and verified their consistency in Figure 4. The importance of this approach is the separation of α and β from EMF without ambiguity. Numerically and analytically verified α and β give us some clues to solve the nonlinear effects neglected in their analytic derivations as well as their experimental application. As long as EMF is represented as $\alpha \overline{\boldsymbol{B}} - \beta \nabla \times \overline{\boldsymbol{B}}$, a negative β replacing the quenching α effect is a necessary condition for the amplification of a large-scale field. Moreover, the negative β effect suppresses the large-scale plasma motion in the helical system. These conclusions are made with semi-analytic equations and simulation data forced with a Gaussian random helical energy. Further, analytical analysis was conducted in a general way that is independent of the forcing method or the fluid system. The method suggested in this manuscript gives as a tool to find the evolving profiles of α and β from externally generated data (simulation or observation).

The physical feature and effect of the helical magnetic field in plasma are useful for investigating the origin of PMF as well as current astrophysical phenomena. The Biermann battery effect shows how the seed magnetic field in the early universe could be generated. Additionally, neutrino–lepton interaction may be a promising candidate for the formation of strong magnetic helicity in the universe. The inverse cascade of magnetic helicity gives us a clue to the expansion of the PMF scale and amplification of its strength. Macroscopically, magnetic helicity explains how the evolution of the magnetic field in plasma is constrained, which eventually leads to the evolution of an astroplasma system. All these events are closely related to HMFD.

In this paper we considered only the case of $Pr_M = 1$ with a fully helical field in HMFD. However, we need to study more general systems with $Pr_M \neq 1$ (e.g., $\sim 10^4$ for an active galactic nucleus disk, $\sim 10^{29}$ for Galaxy cluster) and arbitrary helicity ratios. Moreover, the generation of a poloidal magnetic field from the toroidal field in the solar convection zone with such a low Pr_M ($\sim 10^{-2}$) challenges the current dynamo theory.

The authors acknowledge the support from National Research Foundation of Korea: NRF-2021R1I1A1A01057517, NRF-2020R1A2C3006177, NRF-2021R1A6A1A03043957, and NRF-2020R1F1A1072570.

Appendix

The magnetic induction equation is derived from Faraday's law $\partial \boldsymbol{B}/\partial t = -\nabla \times \boldsymbol{E}$ and Ohm's law:

$$\boldsymbol{E} + \frac{\boldsymbol{U}\times\boldsymbol{B}}{c} - \eta\boldsymbol{J} = \underbrace{\frac{1}{e\rho}\left[\frac{m_e m_i n}{e}\frac{\partial}{\partial t}\left(\frac{\boldsymbol{J}}{\rho}\right) + \frac{(m_i - m_e)}{c}\boldsymbol{J}\times\boldsymbol{B} + m_e\nabla p_i - m_i\nabla p_e + (\boldsymbol{F}_{\rm ex})\right]}_{f_{\rm mag}}. \quad \text{(A1)}$$

This equation is derived from the momentum equation set for the ion–electron plasma. It is modified with various physical conditions before being applied to Faraday's law. In case of $m_i \gg m_e$, the mass-related terms become more simplified. The Hall effect ($\sim m_i/c$) $\boldsymbol{J}\times\boldsymbol{B}$ is neglected if the density of particles is not very high (e.g., a disk in a protostar or dwarf nova). Further, if the (seed) magnetic field exists, the Larmor radius ($mv_\perp/eB$) becomes finite so that the spatially inhomogeneous ∇p_e can be neglected. Moreover, the influence of $\eta\boldsymbol{J}(= m_e\ \nu_c/(ne^{\ 2})\ ne\ (U_i - U_e))$ is ignored if the collision effect ($\nu_c \neq 0$) is trivial. These conditions yield the simplified Ohm's law in the stationary state: $\eta\boldsymbol{J} = \boldsymbol{E} + (1/c)\boldsymbol{U}\times\boldsymbol{B}(c \to 1)$ for the usual MHD equation with kinetic forcing. However, if these conditions are not fulfilled, Ohm's law has additional terms working as a forcing source in the magnetic induction equation. For example, if the (seed) magnetic field is very weak, the Larmor radius grows and ∇p_e plays a dominant role in the amplification of the seed field (Schluter 1950).

$$\boldsymbol{E} + \frac{\boldsymbol{U}\times\boldsymbol{B}}{c} - \eta\boldsymbol{J} = -\frac{\nabla p_e}{en}. \quad \text{(A2)}$$

Then the magnetic induction equation becomes ($c \to 1$)

$$\frac{\partial \boldsymbol{B}}{\partial t} = \nabla\times\langle\boldsymbol{U}\times\boldsymbol{B}\rangle + \frac{\nabla p_e\times\nabla n_e}{n_e^2 e}.\ \left(f_{\rm mag} \to \frac{\nabla p_e}{n_e e}\right). \quad \text{(A3)}$$

This is the typical magnetic forcing dynamo. Moreover, in addition to the Hall effect and the externally provided $\boldsymbol{E}_{\rm ex}$ or $\boldsymbol{B}_{\rm ex}$ from radiation, the abundant lepton–neutrino interaction can be an electromagnetic energy source.

$$\boldsymbol{f} = -\frac{G_F}{\sqrt{2}|e|n_e}\sum_{\nu_a} c_A^a\Big[(n_0^- + n_0^+)\hat{\boldsymbol{b}}\frac{\partial\delta n_{\nu_a}}{\partial t} + (N_0^- + N_0^+)\nabla(\hat{\boldsymbol{b}}\cdot\delta\boldsymbol{j}_{\nu_a})\Big]. \quad \text{(A4)}$$

Its axial vector term is $\boldsymbol{f} = \alpha'\boldsymbol{B}$, where α' is (Semikoz & Sokoloff 2005):[5]

$$\alpha' \sim \frac{ln\ 2}{4\sqrt{2}\pi^2}\left(\frac{10^{-5}T}{m_p^2\lambda^\nu_{\rm fluid}}\right)\frac{\delta n_\nu}{n_\nu}. \quad \text{(A5)}$$

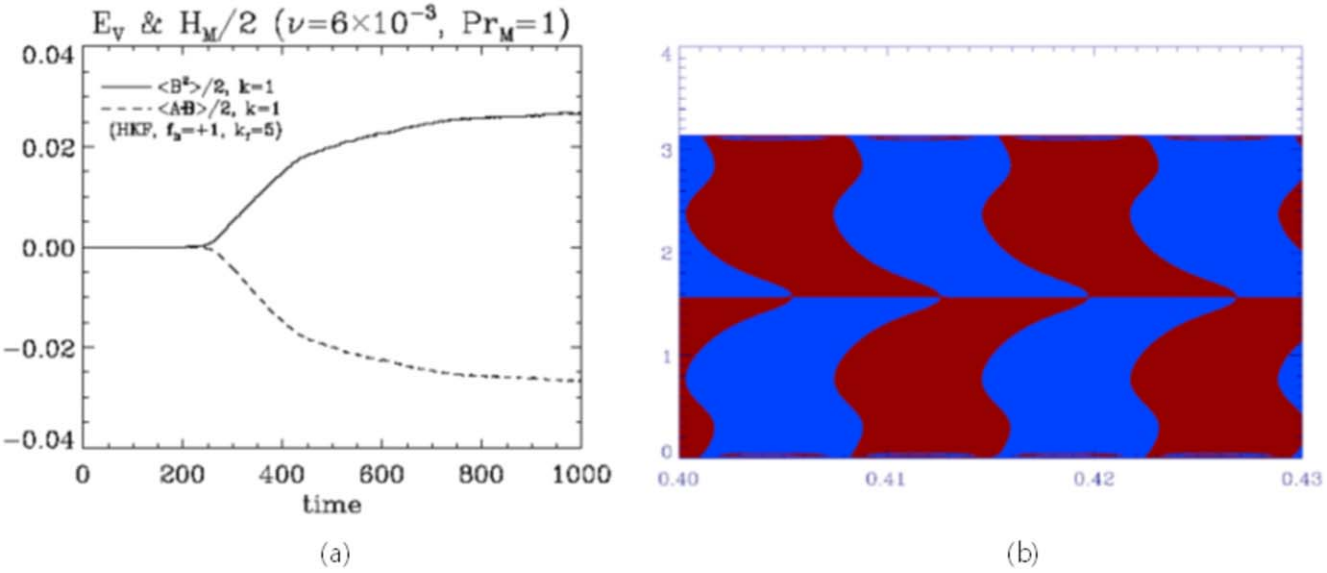

Figure 8. (a) Kinetic helical forcing dynamo (large-scale magnetic field $k = 1$; Equations (3)–(6) with helical $f_{\rm kin}$), which is replaced by α and β. (b) Kinetic helical forcing dynamo derived from Equations (23) and (24). The converted timescale is 21.74 yr.

[5] Fermi constant $G_F = 10^{-5}/m_p^2$(m_p: proton mass); $c_A^a = \mp 0.5$ (axial weak coupling, a: electron, muon, tau; (−): electron, (+)': muon or tau);δn_{ν_a}: neutrino density asymmetry; $\delta\boldsymbol{j}_{\nu_a}$ (neutrino current asymmetry);

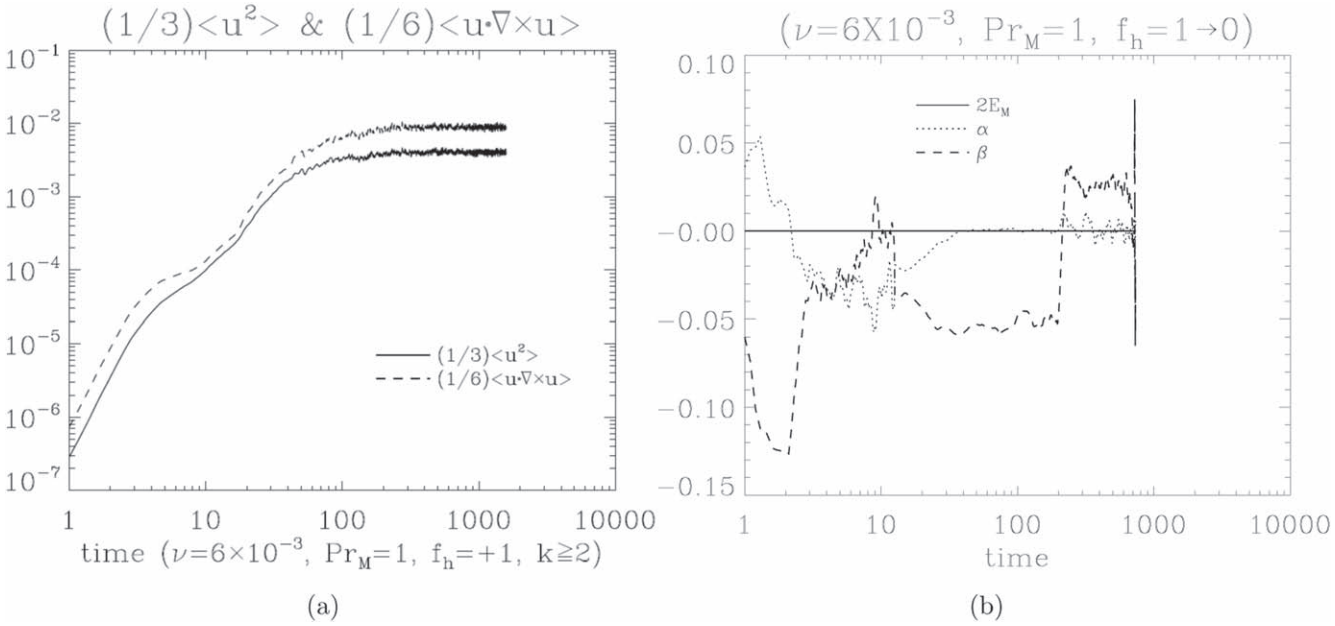

Figure 9. (a) Comparison of the conventional β effect from E_V and that from H_V. All data for $k \geqslant 2$ are summed. (b) Helical kinetic forcing ($H_V \neq 0$) is turned off at $t \sim 200$. The system was continuously driven with nonhelical kinetic energy ($H_V = 0$) Park (2020).

α' is not the same as that of the usual helicity function. However, as it is from the helical interaction $\hat{\boldsymbol{b}} \cdot \delta \boldsymbol{j}_{\nu_a}$, the effect of conserved magnetic helicity can exist in α' (HMFD). The instability of a magnetic field forced by the electron–neutrino asymmetry from a supernova explosion during the first second can produce the (seed) magnetic field of a protostar or a magnetar (Dvornikov & Semikoz 2014).

ORCID iDs

Kiwan Park https://orcid.org/0000-0001-9628-5511
Myung Ki Cheoun https://orcid.org/0000-0001-7810-5134

References

Ahonen, J., & Enqvist, K. 1998, PhRvD, 57, 664
Balbus, S. A., & Hawley, J. F. 1991, ApJ, 376, 214
Biskamp, D. 2005, Magnetic Reconnection in Plasmas (Cambridge: Cambridge Univ. Press)
Biskamp, D. 2008, Magnetohydrodynamic Turbulence (Cambridge: Cambridge Univ. Press)
Boyd, T. J. M., & Sanderson, J. J. 2003, The Physics of Plasmas (Cambridge: Cambridge Univ. Press)
Brandenburg, A. 2001, ApJ, 550, 824
Brandenburg, A., & Kahniashvili, T. 2017, PhRvL, 118, 055102
Brandenburg, A., Kahniashvili, T., & Tevzadze, A. G. 2015, PhRvL, 114, 075001
Brandenburg, A., & Sokoloff, D. 2002, GApFD, 96, 319
Cabanes, S., Schaeffer, N., & Nataf, H.-C. 2014, PhRvL, 113, 184501
Charbonneau, P. 2014, ARA&A, 52, 251
Cheng, B., & Olinto, A. V. 1994, PhRvD, 50, 2421
Davidson, P. A. 2004, in Turbulence: An Introduction for Scientists and Engineers, ed. P. A. Davidson (Oxford: Oxford Univ. Press)
Demozzi, V., Mukhanov, V., & Rubinstein, H. 2009, JCAP, 2009, 025
Ditlevsen, P. D., Jensen, M. H., & Olesen, P. 2004, PhyA, 342, 471
Dvornikov, M., & Semikoz, V. B. 2014, JCAP, 2014, 002
Elsässer, W. M. 1950, PhRv, 79, 183
Galtier, S., Nazarenko, S. V., Newell, A. C., & Pouquet, A. 2000, JPlPh, 63, 447
Giesecke, A., Stefani, F., & Gerbeth, G. 2014, NJPh, 16, 073034
Goldreich, P., & Sridhar, S. 1995, ApJ, 438, 763
Harrison, E. R. 1970, MNRAS, 147, 279
Ichiki, K., Takahashi, K., Ohno, H., Hanayama, H., & Sugiyama, N. 2006, Sci, 311, 827
Kahniashvili, T., Clarke, E., Stepp, J., & Brandenburg, A. 2022, PhRvL, 128, 221301
Kraichnan, R. H. 1976, JFM, 75, 657
Krause, F., & Rädler, K. 1980, Mean-field Magnetohydrodynamics and Dynamo Theory (Oxford: Pergamon Press, Ltd.)
Lanotte, A., Noullez, A., Vergassola, M., & Wirth, A. 1999, GApFD, 91, 131
Lesieur, M. 2008, Turbulence in Fluids (Berlin: Springer)
Luo, Y., Kajino, T., Kusakabe, M., & Mathews, G. J. 2019, ApJ, 872, 172
Machida, M. N., Matsumoto, T., Tomisaka, K., & Hanawa, T. 2005, MNRAS, 362, 369
Maron, J., & Blackman, E. G. 2002, ApJL, 566, L41
Marrelli, L., Martin, P., Puiatti, M. E., et al. 2021, NucFu, 61, 023001
Martin, J., & Yokoyama, J. 2008, JCAP, 2008, 025
McComb, W. D. 1990, The Physics of Fluid Turbulence (Oxford: Clarendon)
Moffatt, H. K. 1978, in Cambridge Monographs on Mechanics and Applied Mathematics, ed. H. K. Moffatt (Cambridge: Cambridge Univ. Press)
Park, K. 2017, PhRvD, 96, 083505
Park, K. 2020, ApJ, 898, 112
Park, K., & Blackman, E. G. 2012a, MNRAS, 419, 913
Park, K., & Blackman, E. G. 2012b, MNRAS, 423, 2120
Park, K., & Cheoun, M.-K. 2022, ApJ, 932, 32
Pouquet, A., Frisch, U., & Leorat, J. 1976, JFM, 77, 321
Schluter, A. 1950, ZNatA, 5, 65
Semikoz, V. B., & Sokoloff, D. 2005, A&A, 433, L53
Subramanian, K. 2016, RPPh, 79, 076901
Tevzadze, A. G., Kisslinger, L., Brandenburg, A., & Kahniashvili, T. 2012, ApJ, 759, 54
Vachaspati, T. 2021, RPPh, 84, 074901
Yamazaki, D. G., Kajino, T., Mathews, G. J., & Ichiki, K. 2012, PhR, 517, 141
Yoshizawa, A. 2011, Hydrodynamic and Magnetohydrodynamic Turbulent Flows (Berlin: Springer)

$n_0^{\pm} \sim (|e|B/2\pi^2)Tln\,2$ is the lepton number density at the Landau level. $\lambda_{\rm fluid}^{\nu} \sim t$ is the scale of the neutrino fluid inhomogeneity.